bioRxiv preprint doi: https://doi.org/10.1101/386516; this version posted August 7, 2018. The copyright holder for this preprint (which was not certified by peer review) is the author/funder, who has granted bioRxiv a license to display the preprint in perpetuity. It is made available under aCC-BY-NC-ND 4.0 International license.

Integrated 'omic' analyses provide evidence that a *Ca.* Accumulibacter phosphatis strain performs denitrification under micro-aerobic conditions

Pamela Y. Camejo[1], *Ben O. Oyserman*[1], *Katherine D. McMahon*[1,2], *Daniel R. Noguera*[1,*]

[1]Department of Civil and Environmental Engineering, University of Wisconsin - Madison, Madison, WI, USA

[2]Department of Bacteriology, University of Wisconsin - Madison, Madison, WI, USA

Email adresses:

camejo.pamela@gmail.com

oyserman@wisc.edu

trina.mcmahon@wisc.edu

noguera@engr.wisc.edu

* Corresponding author: Daniel R. Noguera, 1415 Engineering Drive, Madison, WI 53706. Email: noguera@engr.wisc.edu; Tel: 608-263-7783; Fax: 608-262-5199

bioRxiv preprint doi: https://doi.org/10.1101/386516; this version posted August 7, 2018. The copyright holder for this preprint (which was not certified by peer review) is the author/funder, who has granted bioRxiv a license to display the preprint in perpetuity. It is made available under aCC-BY-NC-ND 4.0 International license.

ABSTRACT

The unique and complex metabolism of *Candidatus* Accumulibacter phosphatis has been used for decades for efficiently removing phosphorus during wastewater treatment in reactor configurations that expose the activated sludge to cycles of anaerobic and aerobic conditions. The ability of Accumulibacter to grow and remove phosphorus during cyclic anaerobic and anoxic conditions has also been investigated as a metabolism that could lead to simultaneous removal of nitrogen and phosphorus by a single organism. However, although phosphorus removal under cyclic anaerobic and anoxic conditions has been demonstrated, elucidating the role of Accumulibacter in this process has been challenging, since experimental research describes contradictory findings and none of the published Accumulibacter genomes show the existence of a complete pathway for denitrification. In this study, we use an integrated omics analysis to elucidate the physiology of an Accumulibacter strain enriched in a reactor operated under cyclic anaerobic and micro-aerobic conditions. The reactor's performance suggested the ability of the enriched Accumulibacter (clade IC) to simultaneously use oxygen and nitrate as electron acceptors under micro-aerobic conditions. A draft genome of this organism was assembled from metagenomic reads (hereafter referred to as Accumulibacter UW-LDO-IC) and used as a reference to examine transcript abundance throughout one reactor cycle. The genome of UW-LDO-IC revealed the presence of a full denitrification pathway. The observed patterns of transcript abundance showed evidence of co-regulation of the denitrifying genes along with a *cbb*$_3$ cytochrome, which is characterized as having high affinity for oxygen, thus supporting the hypothesis that UW-LDO-IC can simultaneously respire nitrate and oxygen. Furthermore, we identified an FNR-like binding motif upstream of the coregulated genes, suggesting transcriptional level regulation of the expression of both denitrifying and respiratory pathways in

bioRxiv preprint doi: https://doi.org/10.1101/386516; this version posted August 7, 2018. The copyright holder for this preprint (which was not certified by peer review) is the author/funder, who has granted bioRxiv a license to display the preprint in perpetuity. It is made available under aCC-BY-NC-ND 4.0 International license.

Accumulibacter UW-LDO-IC. Taken together, the omics analysis provides strong evidence that Accumulibacter UW-LDO-IC simultaneously uses oxygen and nitrate as electron acceptors under micro-aerobic conditions.

IMPORTANCE

Candidatus Accumulibater phosphatis is widely found in full-scale wastewater treatment plants, where it has been identified as the key organism for biological removal of phosphorus. Since aeration can account for 50% of the energy use during wastewater treatment, micro-aerobic conditions for wastewater treatment have emerged as a cost-effective alternative to conventional biological nutrient removal processes. Our study provides strong genomics-based evidence that Accumulibacter is not only the main organism contributing to phosphorus removal under micro-aerobic conditions, but also that this organism simultaneously respires nitrate and oxygen in this environment, consequently removing nitrogen and phosphorus from the wastewater. Such activity could be harnessed in innovative designs for cost-effective and energy-efficient optimization of wastewater treatment systems.

INTRODUCTION

Candidatus Accumulibacter phosphatis (hereafter referred to as Accumulibacter) is the main microorganism removing phosphorus (P) in many wastewater treatment plants performing enhanced biological phosphorus removal (EBPR) (1-4). This uncultured polyphosphate accumulating organism (PAO) fosters a unique and complex metabolism that responds to changes in the availability of carbon, phosphorus, and oxygen. Under anaerobic conditions, Accumulibacter takes up volatile fatty acids (VFA) present in the wastewater and stores the carbon from these simple molecules intracellularly as poly-β-hydroxyalkanoate (PHA), while

bioRxiv preprint doi: https://doi.org/10.1101/386516; this version posted August 7, 2018. The copyright holder for this preprint (which was not certified by peer review) is the author/funder, who has granted bioRxiv a license to display the preprint in perpetuity. It is made available under aCC-BY-NC-ND 4.0 International license.

hydrolyzing intracellular polyphosphate (polyP) to phosphate, which is then released from the cell to the liquid phase (5). The subsequent addition of oxygen into the bulk liquid triggers the use of stored PHA molecules to generate energy for growth, concomitant with the uptake of phosphate from the medium to form polyphosphate, eventually leading to the efficient removal of P from the wastewater.

Analysis of the Accumulibacter lineage has led to the discovery of multiple genome variants. Using the polyphosphate kinase (*ppk1*) gene as a phylogenetic marker, Accumulibacter variants have been subdivided into two types and 14 different clades (types IA-E and IIA-I) (6-9). This genomic divergence may be responsible for observed phenotypic variations of EBPR under different environmental conditions (10-14). Among these differences, Accumulibacter's fitness for anoxic respiration is a topic of much debate since published studies have presented contradictory findings on whether Accumulibacter can respire nitrogenous compounds. While several studies predicted that strains belonging to Accumulibacter type I could use nitrite and/or nitrate as electron acceptors (10, 15-17), other studies concluded that type I is not capable of anoxic nitrate respiration (18, 19). These studies have used different methods for clade classification, with some of them describing Accumulibacter at the type level and others at the clade level, as defined based on *ppk1* phylogeny (6). Therefore, it remains uncertain whether individual clades exhibit a consensus phenotype regarding respiration of nitrogenous compounds. It is also possible that differences in the metabolic potential of Accumulibacter may vary among strains within the same clade. Uncovering the metabolic traits characterizing distinct Accumulibacter populations will provide a better understanding of the ecological role of each of these clades/populations and the biotechnological potential of this lineage in novel nutrient removal processes.

bioRxiv preprint doi: https://doi.org/10.1101/386516; this version posted August 7, 2018. The copyright holder for this preprint (which was not certified by peer review) is the author/funder, who has granted bioRxiv a license to display the preprint in perpetuity. It is made available under aCC-BY-NC-ND 4.0 International license.

In a previous study, we characterized the clade-level population of Accumulibacter in a biological nutrient removal reactor operated under cyclic anaerobic and micro-aerobic conditions and evaluated the ability of the enriched population to use multiple electron acceptors (8). Experimental evidence from this study led to the hypothesis that a particular clade of Accumulibacter (clade IC) could use oxygen and nitrate as electron acceptors (8) when the system is operated with cyclic anaerobic and micro-aerobic conditions. In this study, we use a combination of omics techniques to further investigate the genomic potential, gene expression, and transcriptional regulation of an enriched clade IC Accumulibacter population to further elucidate the metabolic capabilities of this species-like group. This analysis provides strong evidence that the enriched Accumulibacter clade IC population simultaneously uses oxygen and nitrate as electron acceptors under micro-aerobic conditions, and therefore, that this organism contributes to the simultaneous removal of nitrogen and phosphorus from wastewater.

MATERIAL AND METHODS

Operation of Lab-Scale Sequencing Batch Reactor

A laboratory-scale sequencing batch reactor (SBR) was used in this study. The reactor was originally inoculated with activated sludge obtained from the Nine Springs wastewater treatment plant in Madison, WI, which uses a variation of the University of Cape Town (UCT) process designed to achieve biological P removal without nitrate removal (20) and operates with high aeration rates (21). Details of the lab-scale operation under cyclic anaerobic and micro-aerobic conditions are provided in reference (8). Briefly, the SBR had a 2-liter working volume and was fed with synthetic wastewater containing acetate (500 mgCOD/L) as the sole carbon source (C:P molar ratio of 20). The synthetic wastewater was dispensed as two separate media; Media A

bioRxiv preprint doi: https://doi.org/10.1101/386516; this version posted August 7, 2018. The copyright holder for this preprint (which was not certified by peer review) is the author/funder, who has granted bioRxiv a license to display the preprint in perpetuity. It is made available under aCC-BY-NC-ND 4.0 International license.

contained the acetate and phosphate, whereas Media B supplied the ammonia (8). The reactor was operated under alternating anaerobic and low oxygen 8-h cycles. Each cycle consisted of 1.5 h anaerobic, 5.5 h micro-aerobic, 50 min settling and 10 min decanting. During the micro-aerobic stage, an on/off control system was used to limit the amount of oxygen pumped to the reactor (0.02 L/min) and to maintain micro-aerobic conditions in the mixed liquor (DO set point = 0.2 mg/L). The hydraulic retention time (HRT) and solids retention time (SRT) were 24 h and 80 days, respectively. The pH in the system was controlled to be between 7.0 and 7.5.

Sample Collection and Analytical Tests

To monitor reactor performance, mixed liquor and effluent samples were collected, filtered through a membrane filter (0.45 μm; Whatman, Maidstone, UK) and analyzed for acetate, PO_4^{3-}–P, NH_3 + NH_4^+-N, NO_3^--N, and NO_2^--N. The concentrations of PO_4^{3-}–P were determined according to Standard Methods (22). Total ammonia (NH_3 + NH_4^+) concentrations were analyzed using the salicylate method (Method 10031, Hach Company, Loveland, CO). Acetate, nitrite and nitrate were measured using high-pressure liquid chromatography as previously described (8).

For 16S rRNA-based tag sequencing and metagenomic analyses, biomass samples from the reactors were collected weekly and stored at -80°C until DNA extraction was performed. DNA was extracted using UltraClean® Soil DNA Isolation Kit (MoBIO Laboratories, Carlsbad, CA). Extracted DNA was quantified using a NanoDrop spectrophotometer (Thermo Fisher Scientific, Waltham, MA) and stored at -80°C.

For transcriptomic analyses, biomass samples were collected across a single reactor cycle to capture key transition points in the EBPR cycle (Fig. 1). Samples (2 ml) were collected in microcentrifuge tubes, centrifuged, supernatant removed and cell pellets flash frozen in dry ice

bioRxiv preprint doi: https://doi.org/10.1101/386516; this version posted August 7, 2018. The copyright holder for this preprint (which was not certified by peer review) is the author/funder, who has granted bioRxiv a license to display the preprint in perpetuity. It is made available under aCC-BY-NC-ND 4.0 International license.

and ethanol bath within 3 min of collection. RNA was extracted from the samples using a RNeasy kit (Qiagen, Valencia, CA, USA) with a DNase digestion step. RNA integrity and DNA contamination were assessed using the Agilent 2100 Bioanalyzer (Agilent Technologies, Palo Alto, CA, USA).

Ribosomal RNA gene-based Tag sequencing

The composition of the microbial community in the reactor was determined via the analysis of high-throughput sequencing of 16S rRNA gene fragments. The hyper-variable V3–V4 regions of the bacterial 16S rRNA gene were amplified using the primers 515f/806r (23) as described in reference (8). The sequencing data is available under BioProject PRJNA482250. Briefly, PCR products were generated using the Ex Taq kit (Takara); cycling conditions involved an initial 5 min denaturing step at 95°C, followed by 35 cycles at 95°C for 45 s, 50°C for 60 s, 72°C for 90 s, and a final elongation step at 72°C for 10 min. Amplicons were visualized on an agarose gel to confirm product sizes. Purified amplicons were pooled in equimolar quantities and sequenced on an Illumina Miseq benchtop sequencer using pair-end 250 bp kits at the Cincinnati Children's Hospital DNA Core facility.

Paired-end reads obtained were merged, aligned, filtered and binned into operational taxonomic units (OTU) with 97% identity using the QIIME pipeline (24). Chimeric sequences were removed using UCHIME (25). The most representative sequences from each OTU were taxonomically classified using the MIDas-DK database (26).

Quantitative polymerase chain reaction (qPCR)

Quantification of each Accumulibacter clade was carried out by qPCR using a set of clade-specific primers targeting the polyphosphate kinase (*ppk1*) gene (8). All qPCR reactions were run in a LightCycler 480 system (Roche applied Science, Indianapolis, IN). Each reaction

bioRxiv preprint doi: https://doi.org/10.1101/386516; this version posted August 7, 2018. The copyright holder for this preprint (which was not certified by peer review) is the author/funder, who has granted bioRxiv a license to display the preprint in perpetuity. It is made available under aCC-BY-NC-ND 4.0 International license.

volume was 20 µL and contained 10 µL iQ™ SYBR® Green Supermix (BioRAD Laboratories, Hercules, CA), 0.8 µL each of 10 µM forward and reverse primer, 4.4 µL nuclease free water and 4 µL of sample. Templates for qPCR were obtained from clone collections or gene synthesis (IDT, USA). In all cases, ten-fold serial dilutions of each template (ranging from 10^1 to 10^7 copies per reaction) were used to generate qPCR calibration curves. All samples were processed in triplicate and each reaction plate contained non-template controls.

Metagenome sequencing, assembly and binning

Samples from days 522 and 784 were selected for metagenomic analysis. Illumina TruSeq DNA PCR free libraries were prepared for DNA extracts according to the manufacturer's protocol and paired-end sequenced on either the Illumina HiSeq 2000 platform (v4 chemistry, 2 × 150 bp; 522-day sample), or the Illumina MiSeq platform (v3 chemistry, 2 × 250 bp; 784-day sample). A sample from day 522 was also sequenced on MinION (Oxford Nanopore Technologies, Oxford, UK), according to the Oxford Nanopore Genomic DNA Sequencing protocol (SQK-MAP003). The MinION flowcell was run for 48-h using the MinION control software, MinKNOW (version 47.3) and online base-calling was performed by the software Metrichor (version 2.23). Raw reads have been submitted to NCBI and are accessible under the BioProject identifier PRJNA322674.

Illumina unmerged reads were quality-trimmed and filtered with Sickle (https://github.com/ucdavis-bioinformatics/sickle.git), using a minimum phred score of 20 and a minimum length of 50 bp. Metagenomic reads from day 522 were assembled using the metaSPAdes pipeline of SPAdes 3.9.0 (27) and individual genome bins were extracted from the metagenome assembly using MaxBin (28). Genome completeness and redundancy was estimated using CHECKM 0.7.1 (29). Taxonomic identity of the bins was assigned using PhyloSift v 1.0.1

bioRxiv preprint doi: https://doi.org/10.1101/386516; this version posted August 7, 2018. The copyright holder for this preprint (which was not certified by peer review) is the author/funder, who has granted bioRxiv a license to display the preprint in perpetuity. It is made available under aCC-BY-NC-ND 4.0 International license.

(30) and the script 'parse_phylosift_sts.py' available at https://github.com/sstevens2/sstevens_pubscrip/blob/master/parse_phylosift_sts.py (with options *-co_prob* 0.7 and *-co_perc* 0.7). Bin information is summarized in Table S1.

Two putative Accumulibacter bins (bin.046 and bin.097.4 in Table S1) were identified. The bin with the highest completeness (bin.046; hereafter referred to as UW-LDO-IC) was selected for further analysis and subjected to further processing to improve its quality. Redundant scaffolds were manually removed based on tetra-nucleotide frequency and differential coverage, using metagenomic reads from days 522 and 784 and following the anvi'o workflow described in A. M. Eren et al. (31). Further scaffolding was performed on UW-LDO-IC using Nanopore long-reads and the LINKS algorithm (32). Gapcloser (https://sourceforge.net/projects/soapdenovo2/files/GapCloser/) was used for additional gap filling. Table S2 displays quality metrics of the Accumulibacter draft genome after each of the steps previously described. The metagenomic assembly and final Accumulibacter bin was annotated using MetaPathways v 2.0 (33) and can be found under the GenBank accession number QPGA00000000.

Average Nucleotide Identity (ANI)

Pair-wise ANI values of Accumulibacter genomes were obtained using the ANIm method (34) and implemented in the Python script 'calculate_ani.py' available at https://github.com/ctSkennerton/scriptShed/blob/master/calculate_ani.py.

Phylogenetic Analyses

The phylogeny of Accumulibacter UW-LDO-IC was assessed by constructing a phylogenetic tree using a concatenated alignment of marker genes. Published Accumulibacter

bioRxiv preprint doi: https://doi.org/10.1101/386516; this version posted August 7, 2018. The copyright holder for this preprint (which was not certified by peer review) is the author/funder, who has granted bioRxiv a license to display the preprint in perpetuity. It is made available under aCC-BY-NC-ND 4.0 International license.

draft and complete genomes were included in the analysis. First, PhyloSift was used to extract a set of 38 marker genes from each genome. Then, the extracted marker protein sequences were concatenated into a continuous alignment to construct a maximum-likelihood (ML) tree, using RAxML v 7.2.8 (35). RAxML generated 100 rapid bootstrap replicates followed by a search for the best-scoring ML tree.

For phylogenetic analyses of the polyphosphate kinase 1 (*ppk1*), nitrate reductase alpha subunit (*narG*), nitrite reductase (*nirS*), nitric oxide reductase (*norZ*), and nitrous oxide reductase (*nosZ*) genes, nucleotide datasets were downloaded from the NCBI GenBank database (36). Alignments were performed using the 'AlignSeqs' command in the DECIPHER "R" package (37). Phylogenetic trees were calculated using neighbor-joining criterion with 1,000 bootstrap tests for every node and the trees were visualized with the assistance of FigTree v1.4 (http://tree.bio.ed.ac.uk).

RNA sequencing, filtering and mapping

Six biomass samples from within a reactor cycle on operational day 522 (Fig. 1) were collected and immediately processed to determine transcript abundance. RNA was extracted from the samples using a RNeasy kit (Qiagen, Valencia, CA, USA) with a DNase digestion step. RNA integrity and DNA contamination were assessed using the Agilent 2100 Bioanalyzer (Agilent Technologies, Palo Alto, CA, USA). Ribosomal RNA (rRNA) was removed from 1 µg of total RNA using Ribo-Zero rRNA Removal Kit (Bacteria) (Epicentre, Madison, WI, USA). Libraries were generated using the Truseq Stranded mRNA sample preparation kit (Illumina, San Diego, CA, USA), according to the manufacturer's protocol. The libraries were quantified using KAPA Biosystem's next-generation sequencing library quantitative PCR kit and run on a Roche LightCycler 480 realtime PCR instrument. The quantified libraries were then prepared for

bioRxiv preprint doi: https://doi.org/10.1101/386516; this version posted August 7, 2018. The copyright holder for this preprint (which was not certified by peer review) is the author/funder, who has granted bioRxiv a license to display the preprint in perpetuity. It is made available under aCC-BY-NC-ND 4.0 International license.

sequencing on the Illumina HiSeq 2000 sequencing platform utilizing a TruSeq paired-end cluster kit, v3, and Illumina's cBot instrument to generate a clustered flowcell for sequencing. Sequencing of the flowcell was performed on the Illumina HiSeq 2000 sequencer using a TruSeq SBS sequencing kit 200 cycles, v3, following a 2×150 indexed run recipe. Sequence data were deposited at IMG/M under Taxon Object IDs 3300004259-3300004260 and 3300004621-3300004624.

RNA reads were quality filtered and trimmed with Sickle and forward and reverse reads were merged using FLASH (v. 1.2.11) (38). Ribosomal RNA sequences were removed with SortMeRNA using six built in databases for bacterial, archaeal and eukaryotic small and large subunits (39). Reads that passed filtering were then mapped to the metagenomic assembly and to the complete and draft genomes using the BBMap suite (40) with default parameters, respectively. Read counts were then calculated using HTseq with the 'intersection strict' parameter (41). Read counts were normalized by total reads in the sequencing run, the number of reads that remained after rRNA filtering, and the fraction of total reads that aligned to the assembly and genomes (Table S3) in each sample. Number of reads mapping to each gene were then converted to $\log_2$ reads per kilobase per million (RPKM (42)).

Primer design

PCR primer sets targeting the Accumulibacter UW-LDO-IC's genes *nirS*, *narG*,, *norZ*, *nosZ*, the *ccoN* subunit of *cbb3* and the *ctaD* subunit of *caa3* cytochrome oxidases, were designed to quantify expression of these genes in cDNA samples from the reactor. For comparison, primers for the *rpoN* gene were also designed (Table S4). For primer design, genes from UW-LDO-IC and other published Accumulibacter genomes were aligned with homologs from bacteria that share relatively high DNA sequence identity with Accumulibacter. The list of aligned gene

bioRxiv preprint doi: https://doi.org/10.1101/386516; this version posted August 7, 2018. The copyright holder for this preprint (which was not certified by peer review) is the author/funder, who has granted bioRxiv a license to display the preprint in perpetuity. It is made available under aCC-BY-NC-ND 4.0 International license.

sequences was then submitted to DECIPHER's Design Primers web tool (43) using the following parameters: primers length ranging from 17-26 nucleotides with up to 2 permutations and PCR product amplicon length between 75-500 bp.

PCR amplification of UW-LDO-IC gene fragments was carried out on extracted genomic DNA from the lab-scale SBR, in a 25 μL reaction volume with 400 nM of each forward and reverse primer. The PCR program consisted of an initial 10-min denaturation step at 95°C, followed by 30 cycles of 95°C for 30 s, 64°C for 30 s, and 72°C for 30 s, and then a final extension at 72°C for 5 min. The presence and sizes of the amplification products were determined by agarose (2%) gel electrophoresis of the reaction product. The amplified fragments were then purified, cloned using a TOPO TA cloning kit (Invitrogen, CA) according to the manufacturer's instructions. Fragments were single-pass Sanger sequenced, and the sequences were aligned to Accumulibacter UW-LDO-IC to confirm specificity. In all cases, PCR fragment sequences aligned to the corresponding gene in UW-LDO-IC with a percent of identity > 97%, whereas the identity percentage with other Accumulibacter genomes was < 95%. The sequences have been deposited in GenBank under BioProject PRJNA482254.

Quantitative real-time PCR

Complementary DNA (cDNA) was generated from 500 ng of total RNA, primed by random hexamers (SuperScript II first-strand synthesis system, Invitrogen, Carlsbad, CA, USA). The reaction was terminated by incubation at 85^{o}C for 5 min and RNase H treatment was performed to degrade RNA in RNA:DNA hybrids. Subsequently, 4 μL of 10x diluted cDNA was applied as the template in qPCR. All quantifications were performed in triplicate. The qPCR was conducted on a LightCycler 480 (Roche, Switzerland) using iQ SYBR Green Supermix (Bio-Rad) with a total reaction volume of 20 μL. All qPCR programs consisted of an initial 3 min denaturation at

bioRxiv preprint doi: https://doi.org/10.1101/386516; this version posted August 7, 2018. The copyright holder for this preprint (which was not certified by peer review) is the author/funder, who has granted bioRxiv a license to display the preprint in perpetuity. It is made available under aCC-BY-NC-ND 4.0 International license.

95°C, followed by 45 cycles of denaturing at 95°C for 30 s, 64°C for 30 s, and 72°C for 30 s. RNA samples without reverse transcription were used as no RT (reverse transcription) controls to evaluate DNA contamination for all primers tested. The relative fold change of target gene expression between samples was quantified using Accumulibacter *rpoN* as a reference gene.

Operons and upstream motif identification

De novo motif detection analysis was conducted on the intergenic regions upstream of the *nar*, *nir*, *nor*, *nos*, *caa3* and *cbb3* operons of Accumulibacter UW-LDO-IC using MEME (44). FNR-motif sites were further identified in both strands of other Accumulibacter genomes using the FIMO tool (45) (p-values < 1×10^{-5}). Search was limited to the promoter region, represented by the 300 bp intergenic region upstream of the transcriptional start site, of all protein-coding sequences annotated with MetaPathways (33).

Putative operons were determined using the same set of criteria as in reference (46). That is, each operon enclosed adjacent genes with the same orientation, co-expressed with a minimum Pearce correlation coefficient of 0.7, and an intergenic region between genes of 1000 base pairs or less.

RESULTS AND DISCUSSION

Characterization of reactor operation and Accumulibacter community structure

A nutrient profile of one reactor's cycle from the date samples were collected for transcriptomics (day 522) is shown in Fig. 1. Acetate was slowly added to the reactor during the first 32 minutes of the anaerobic phase, with no accumulation observed, as it was rapidly consumed. P release to the mixed-liquor was observed during the period of acetate uptake. During the anaerobic stage, ammonia-containing media was supplied during the first 16 min of

bioRxiv preprint doi: https://doi.org/10.1101/386516; this version posted August 7, 2018. The copyright holder for this preprint (which was not certified by peer review) is the author/funder, who has granted bioRxiv a license to display the preprint in perpetuity. It is made available under aCC-BY-NC-ND 4.0 International license.

the anaerobic stage and the ammonia accumulated in the reactor. In the micro-aerobic phase, when measured DO was about 0.02 mg/L, P was taken up by cells. Simultaneously, nitrification occurred during the first 3 hours of aeration, without NO_2^- or NO_3^- accumulation, indicating simultaneous nitrification and denitrification in the reactor. After all the substrates that exert oxygen demand were depleted, oxygen increased and fluctuated around the 0.2 mg/L set point. These observations are consistent with an efficient EBPR process under cyclic anaerobic and micro-aerobic conditions, as discussed elsewhere (8).

Samples collected on the same day for 16S rRNA amplicon sequencing indicated that Accumulibacter was the most abundant bacterium in the reactor, accounting for 34% of the total number of reads (Table S5). Members of the *Competibacteraceae* family (16%) and the *Lewinella* genus (11%) were also abundant. The diversity within the Accumulibacter lineage was assessed by qPCR (Table S6). In these samples the Accumulibacter members were dominated by Clade IC, which accounted for 74% of the total, followed by Clade IID (14%) and IIA (9%). As described before (8), clade IC predominated in the reactor during at least 300 days of operation, with abundances greater than 87% of total Accumulibacter, and batch tests suggested its ability to use oxygen, nitrite, and nitrate as electron acceptors (8). Clade IC has also been described as the dominant Accumulibacter clade in a reactor operated under anaerobic/anoxic/oxic conditions (18). However, contrary to our findings, batch tests suggested that this strain was not capable of using nitrate as external electron acceptor for anoxic P-removal. This inconsistency among denitrifying capabilities could be the result of genetic variations that are not captured with the current *ppk1*-based clade definitions.

Assembling a draft genome of Accumulibacter clade IC

bioRxiv preprint doi: https://doi.org/10.1101/386516; this version posted August 7, 2018. The copyright holder for this preprint (which was not certified by peer review) is the author/funder, who has granted bioRxiv a license to display the preprint in perpetuity. It is made available under aCC-BY-NC-ND 4.0 International license.

All existing metagenome assembled genomes (MAGs) of Accumulibacter have been obtained from bioreactors operated under conventional anaerobic/aerobic cycles that use abundant aeration (47-50). To date, only one genome of Accumulibacter has been closed (clade IIA strain UW-1), while draft genomes from 5 different clades (clade IA, IB, IIA, IIC and IIF) have been reconstructed from metagenomic data. Since the SBR reactor operated with anaerobic/micro-aerobic cycles enriched for a less common clade of Accumulibacter, we performed a metagenomic assessment of the microbial community in the reactor. The whole-community DNA of two samples from the reactor were sequenced using two different technologies: Illumina and Oxford Nanopore. Short Illumina reads were initially assembled and binned into 136 different bacterial draft genomes (Table S1). One of these bins was classified as Accumulibacter (bin.046) and characterized by its high completeness (94.8%) and relatively high redundancy (28.9%), likely due to the presence of redundant gene markers from other Accumulibacter strains. The presence of another incomplete bin also classified as Accumulibacter (bin.097.4; 26.0% completeness) further support the idea of other Accumulibacter strains present at lower concentrations, in agreement with the assessment of diversity based on the *ppk1* gene (Table S6). To obtain a higher-quality draft genome of the dominant Accumulibacter strain, the differential coverage of two metagenomic samples was used to remove contaminant contigs, reducing the redundancy level to 0.84% of marker genes. Finally, Nanopore sequencing data was used for further scaffolding; gaps were filled using the GapCloser tool. The resulting near-complete draft genome, termed Accumulibacter sp. UW-LDO-IC, has 4.7 Mbp in total with average GC content of 62.5% (Table S2) and encoded 95.2% of marker genes with 0.68% redundancy.

bioRxiv preprint doi: https://doi.org/10.1101/386516; this version posted August 7, 2018. The copyright holder for this preprint (which was not certified by peer review) is the author/funder, who has granted bioRxiv a license to display the preprint in perpetuity. It is made available under aCC-BY-NC-ND 4.0 International license.

A phylogenetic tree constructed from the *ppk1* gene encoded in UW-LDO-IC, other Accumulibacter genomes and sequences available at NCBI, were used to classify UW-LDO-IC into one of the 14 Accumulibacter clades described to date. According to the phylogenetic tree topology of the *ppk1* gene (Fig. 2A), UW-LDO-IC's *ppk1* clustered with sequences previously classified as clade IC, and therefore, the draft genome assembled herein would belong to this clade. With more Accumulibacter draft genomes becoming available in recent years, the tree topology also suggests that Accumulibacter BA-92 (49), a draft genome initially classified as clade IC may be better classified as belonging to clade IB along with the draft genome HKU-1 (48). To further evaluate this potential misclassification, a phylogenetic tree of a concatenated protein alignment of 38 universally distributed single-copy marker genes (51) was constructed (Fig. 2B). This tree topology supports the classification of UW-LDO-IC as belonging to Type I, but separate from Accumulibacter BA-92 and HKU-1. Thus, we propose that UW-LDO-IC be classified as the only draft genome representing clade IC, and Accumulibacter BA-92 and HKU-1 be classified in clade IB, along with Accumulibacter UBA2783 (52).

Average nucleotide sequence identity (ANI) between UW-LDO-IC and formerly published Accumulibacter genomes was used to confirm the phylogenetic analysis, as this method has been shown to correlate well with previously defined species boundaries (53, 54). The calculated ANI and alignment fraction for the Accumulibacter genomes showed that UW-LDO-IC shares only 88.7 and 88.3% identity and 67.2 and 60.2% alignment with Accumulibacter HKU-1 (Clade IB) and BA-92 (Clade IB), respectively (Fig. S1). The low ANI and low alignment, as well as the concatenated markers phylogeny, indicates that Accumulibacter UW-LDO-IC has significant differences with other Accumulibacter genomes, none of which have been retrieved from BNR microbiomes adapted to minimal aeration.

bioRxiv preprint doi: https://doi.org/10.1101/386516; this version posted August 7, 2018. The copyright holder for this preprint (which was not certified by peer review) is the author/funder, who has granted bioRxiv a license to display the preprint in perpetuity. It is made available under aCC-BY-NC-ND 4.0 International license.

372 **Denitrification potential of Accumulibacter UW-LDO-IC**

373 A comparison of the genetic inventory involved in anoxic respiration revealed differences
374 between UW-LDO-IC and previously published Accumulibacter genomes (Table 1 and S7).
375 Among the differences found is that UW-LDO-IC encodes a full denitrification pathway, which
376 involves a membrane bound nitrate reductase of the NarG type (*narGHJI* operon), as well as a
377 nitrate/nitrite transporter homologous to the *narK* gene, a periplasmic cytochrome cd_1 nitrite
378 reductase NirS and the proteins involved in heme d_1 biosynthesis (*nirMCFDLGHJN*), a quinol-
379 dependent nitric oxide reductase *norZ* and a nitrous oxide reductase Nos (*nosZDFYL*) (Table 1).
380 The genetic context of these genes was compared to other Accumulibacter genomes (Fig. S2).
381 The position of denitrifying genes within the genome varied among different clades. Overall,
382 genes flanking the *nar* operon, *nirS-2* and *nosZ* genes were the same in all Accumulibacter
383 clades where these genes were identified, including UW-LDO-IC. Unlike clade IIC or IB, *nirS-1*
384 of UW-LDO-IC was not positioned next to the *nar* or *nor* genes, but the genomic context of
385 *nirS-1* in UW-LDO-IC differed from any Accumulibacter genome. Since *nirS-1* from UW-LDO-
386 IC presented high identity with Accumulibacter HKU-1 and BA-92 (91%), this difference in the
387 genome context might be caused by lateral gene transfer. The presence of transposase genes next
388 to *uspA* in BA-93 (a flanking gene of *nirS-1* in UW-LDO-IC (Fig. S2)) supports this hypothesis.
389 An alignment of full-length sequences of subunits *narG*, *nirS*, *norZ* and *nosZ*, which
390 contain the active sites in the corresponding enzymes, was used to evaluate the phylogenetic
391 associations of these genes (Fig. S3-S6). This analysis revealed that all UW-LDO-IC genes
392 involved in denitrification were closely related to other members of the Accumulibacter genus,
393 ruling out possible contig contamination from other denitrifying bacteria during binning.
394 Phylogenetic differentiation between genes belonging to type I and II of Accumulibacter was

bioRxiv preprint doi: https://doi.org/10.1101/386516; this version posted August 7, 2018. The copyright holder for this preprint (which was not certified by peer review) is the author/funder, who has granted bioRxiv a license to display the preprint in perpetuity. It is made available under aCC-BY-NC-ND 4.0 International license.

observed, where genes belonging to UW-LDO-IC clustered with other genes from type I genomes. In the case of *narG*, which has only been identified in genomes from clade IIC, UW-LDO-IC clustered separatedly from the Clade II genes (Fig. S3).

Denitrifying genes encoded in Accumulibacter genomes were phylogenetically related to different taxonomic groups. Genes encoding the NarG proteins seem to have derived from other *Betaproteobacteria*. Interestingly, these genes exhibit phylogenetic relation with *narG* from different bacterial families (*Comamonadaceae, Pseudomonaceae, Burkholderaceae and Rhodocyclaceae*), indicating a similar origin (Fig. S3). The close relationship of Accumulibacter's *narG* with the plasmid-encoded gene in *Burkholderia phymatum* suggests potential mobility of this gene across genera.

Multiple copies of *nirS* are present in the majority of Accumulibacter genomes, including UW-LDO-IC (Fig. S4). The phylogenetic analysis of sequences encoding this gene indicates two main clusters of *nirS* including sequences from both Accumulibacter and other members of the *Rhodocylaceae* family, with one of these clusters, harboring the *nirS-2* and *nirS-3* genes of UW-LDO-IC, being closely related to sequences from the *Pseudomonas* genus. Interestingly, no other *Rhodocyclaceae* member encoded a quinol-dependent nitric oxide reductase (*norZ*), since in these species, nitric oxide reduction requires the activity of a cytochrome *bc*-type complex (*norBC*). Accumulibacter's *norZ* was instead phylogenetically most closely related to *Polaromonas*, another member of the *Comamonadaceae* family (Fig. S5). Finally, the closest sequences to Accumulibacter's *nosZ* gene, belonged to the *Dechloromonas* (*Rhodocyclaceae* member) (Fig. S6). These findings are in agreement with a recent ancestral genome reconstruction and evolutionary analysis of the Accumulibacter lineage, which found that the denitrification machinery was not present in the last common ancestor of Accumulibacter and

bioRxiv preprint doi: https://doi.org/10.1101/386516; this version posted August 7, 2018. The copyright holder for this preprint (which was not certified by peer review) is the author/funder, who has granted bioRxiv a license to display the preprint in perpetuity. It is made available under aCC-BY-NC-ND 4.0 International license.

that one of the most abundant source of horizontally transferred genes are the *Burkholderiales*, including many from *Comamonadaceae* (see Supplementary Table 6 in reference (55)). Overall, these results suggest that part of the denitrification machinery of Accumulibacter was laterally transferred from other microorganisms commonly found in activated sludge.

Only incomplete denitrification pathways, with the potential of reducing nitrite to nitrogen gas (Accumulibacter UW-1, UBA6658, UBA2783, UW-2, BA-92 and BA-93) and nitrate to nitric oxide (Accumulibacter SK-01, SK-02, BA-91, UBA5574 and HKU-2), were identified in other Accumulibacter genomes (Table 1). Furthermore, evidence for a periplasmic nitrate reductase Nap enzyme was not found in UW-LDO-IC but is present in other Accumulibacter genomes (Table 1). Although it has been hypothesized that Nap could be responsible for the nitrate reduction step in some Accumulibacter strains (49), due to the functional diversity of this enzyme, involved in denitrification, nitrate reduction to ammonia, maintenance of cellular oxidation–reduction potential and nitrate scavenging, the presence of a *nap* homolog in an organism's genome cannot necessarily be linked to nitrate respiration (56). For instance, despite the existence of a *nap* operon within the Accumulibacter UW-IA (clade IIA) genome (Table 1 and S7), J. J. Flowers et al. (10) demonstrated through batch denitrification assays, that this strain could not use nitrate as a terminal electron acceptor. Therefore, UW-LDO-IC would be the first Accumulibacter genome found to encode a full denitrifying machinery, containing genes directly involved in the reduction of nitrate to nitrogen gas, settling a long-running debate in the research community about whether Accumulibacter can achieve complete nitrate reduction to nitrogen gas while cycling polyphosphate (10, 15, 17, 57).

Aerobic respiration potential of Accumulibacter UW-LDO-IC

bioRxiv preprint doi: https://doi.org/10.1101/386516; this version posted August 7, 2018. The copyright holder for this preprint (which was not certified by peer review) is the author/funder, who has granted bioRxiv a license to display the preprint in perpetuity. It is made available under aCC-BY-NC-ND 4.0 International license.

The presence of known terminal oxidases, which catalyze oxygen reduction to water during the final step of the electron transport chain (58), was examined in the available Accumulibacter genomes. Three known terminal oxidases were annotated in all genomes of Accumulibacter: cytochrome aa_3 (encoded by the *ctaDCE*), ba_3 (encoded by the subunits *cbaA and cbaB*) and cbb_3 (encoded by operon *ccoNOQP*) oxidases, which accept electrons from cytochrome c and transfer them in reactions involved in oxygen reduction (Table 2 and S8). The aa_3-type oxidases have low affinity for oxygen and usually play a dominant role under high oxygen conditions (59-61). Phylogeny of the first subunit of this enzyme (Fig. S7) shows marked differentiation of the Accumulibacter lineage from other *Rhodocyclaceae* organisms, although some genomes of Accumulibacter, including UW-I (clade IIA), clustered closely to *Dechloromonas*. All genomes classified as clade IIF lacked this subunit (Table 2), and thus, members of this group might rely on other cytochrome c oxidases for aerobic respiration.

On the other hand, cbb_3 oxidases are known to have very high affinity for oxygen and to be induced under low oxygen conditions in many bacteria (62-66). This enzyme is widespread in the Accumulibacter lineage, since 18 out of the 21 genomes analyzed herein harbored the *cco* operon encoding the subunits of this enzyme (Table 2). These results indicate that the ability to survive in low-oxygen concentrations is common across Accumulibacter strains and would explain why lowering oxygen concentration does not seem to negatively affect EBPR (8, 21, 67). The phylogenetic analysis of the first subunit of this enzyme, *ccoN*, shows conservation of this trait among members of the *Rhodocyclaceae* family (Fig. S8).

Lastly, ba_3-type cytochrome oxidase has been mostly studied in the extremophile bacterium *Thermus thermophilus,* where it is usually expressed under oxygen limiting conditions (68), but little is known about its role in other organisms. In Accumulibacter this enzyme is

bioRxiv preprint doi: https://doi.org/10.1101/386516; this version posted August 7, 2018. The copyright holder for this preprint (which was not certified by peer review) is the author/funder, who has granted bioRxiv a license to display the preprint in perpetuity. It is made available under aCC-BY-NC-ND 4.0 International license.

present in all clades (Table 2) and its phylogeny reveals that it could be derived from non-*Rhodocyclaceae* members (Fig. S9).

Changes in transcript abundance during an anaerobic/micro-aerobic cycle

Transcriptional investigations in Accumulibacter have illuminated how the complex and unique metabolism of this lineage is a result of highly dynamic gene expression (46, 48, 69, 70). Recently, the power of time series metatranscriptomics was used to analyze gene expression patterns in Accumulibacter during an anaerobic-aerobic EBPR cycle (46). This study was carried out with high oxygen concentrations in a reactor where nitrification was inhibited and anoxic respiration did not take place. In order to study the effect of limited oxygen conditions in the expression of the respiratory machinery of Accumulibacter UW-LDO-IC, we used a similar time series high-resolution RNA-seq approach and contrasted the effect of high/low oxygen in the metabolism of this strain.

A time-series metatranscriptomic dataset of the lab-scale reactor was obtained in collaboration with DOE-JGI. Samples were collected at the beginning of the anaerobic stage and at different times during the micro-aerobic stage when DO conditions were ~0.05 mg/L and 0.25 mg/L, respectively (Fig. 1). RNA sequencing resulted in 1,718,478,214 total reads across the six samples (Table S3). Quality filtering, merging, and rRNA removal resulted in 396,995,401 sequences for downstream analysis. Resulting reads were then competitively mapped to Accumulibacter UW-LDO-IC and other publicly available Accumulibacter complete and draft genomes, including clades IA, IB, IIA, IIC and IIF (Table S9). Between 48-50% of each sample's filtered RNA reads mapped to the genome of UW-LDO-IC, indicating that this was the most active bacterium in the community. No other genome of Accumulibacter retrieved more

bioRxiv preprint doi: https://doi.org/10.1101/386516; this version posted August 7, 2018. The copyright holder for this preprint (which was not certified by peer review) is the author/funder, who has granted bioRxiv a license to display the preprint in perpetuity. It is made available under aCC-BY-NC-ND 4.0 International license.

485 than 0.52% of mapping reads, and therefore, strains closely related to other available
486 Accumulibacter genomes were not active members of the community.

487 Transcripts mapping to genes related to denitrification were investigated by analyzing
488 Accumulibacter UW-LDO-IC gene expression patterns during the cycle. Fig. 3 depicts the
489 relative expression of genes encoding the *nar*, *nir*, *nor* and *nos* operons, and nitrite-nitrate
490 transporters (*narK*) at each time point; the minimum expression of each gene was subtracted
491 from each point to allow better visualization of the dynamics of each gene over the course of the
492 cycle. All subunits of the *narGHJI* operon showed similar patterns, with transcript abundance
493 increasing during the anaerobic stage, followed by a decrease in transcript levels as the oxygen
494 concentration increased in the system at the end of the cycle (Fig. 3A). Only one of the three
495 *nirS* copies (*nirS*-1) present in Accumulibacter UW-LDO-IC showed an increment on its
496 transcript abundance during the cycle (maximum $\Delta\log_2$(RPKM) read count >1), with a pattern
497 similar to that of the *narGHJI operon* (Fig. 3B). Transcripts from the *narK* and *nosZ* genes also
498 increased during the anaerobic stage, but their abundance started decreasing as soon as air was
499 introduced to the reactor (Fig. 3D-E). The gene *norZ* did not display a notable change in relative
500 transcript abundance (maximum $\Delta\log_2$(RPKM) read count < 1), although its expression increased
501 over time (Fig. 3C). These observations are consistent with upregulation of denitrifying genes
502 during the anaerobic stage, suggesting that oxygen concentration plays an important role in
503 transcriptional regulation of these genes, as has been previously described (71).

504 Similar transcript trends for denitrification-associated genes have been previously
505 described in Accumulibacter, in reactors operating with anaerobic/aerobic cycles that used high
506 aeration rates and where nitrification was chemically inhibited with allylthiourea (46, 69). In
507 general, these studies showed upregulation of denitrification genes during anaerobic conditions

bioRxiv preprint doi: https://doi.org/10.1101/386516; this version posted August 7, 2018. The copyright holder for this preprint (which was not certified by peer review) is the author/funder, who has granted bioRxiv a license to display the preprint in perpetuity. It is made available under aCC-BY-NC-ND 4.0 International license.

and a reduction in transcript abundance when oxygen was introduced to the system. However, unlike the results observed at high-DO (46), our observations indicate that transcript abundance remains high after oxygen addition, when simultaneous nitrification/denitrification is occurring. The *norZ* gene expression pattern under low-oxygen also differs from the one reported at high-DO (46), since the transcripts of this gene in UW-LDO-IC did not considerably change during the aerobic period, whereas transcripts in UW-1 exhibited high variations during the operational cycle (Fig, 4B). Furthermore *nosZ* transcript levels under oxygen-limited conditions displayed a slower decrement rate than what was reported at high-DO (46), where negligible expression was observed after 1 hour of aeration, and similar results were described in S. M. He and K. D. McMahon (69) (Fig, 4C). Since the complete denitrification pathway was not present in the Accumulibacter UW-1 genome, no information about *nar* operon expression was available prior to our study.

Previous studies have confirmed Accumulibacter's capability to synthesize denitrification-associated proteins. In J. J. Barr et al. (47), nitrite and nitrous oxide reductase enzymes were detected by metaproteomic analysis of an Accumulibacter-enriched microbial community. No nitric oxide reductase protein was detected in this study, despite the presence of the gene *norZ i*n the genome of the strain enriched in this system, Accumulibacter BA-93 (IA). As observed in Fig. 3C, *norZ* transcript levels in UW-LDO-IC did not considerably changed over time, potentially indicating a low transcriptional level response to changes in oxygen or nitrite/nitrate concentrations, hence other regulatory mechanisms might control synthesis of this enzyme. Further experiments are still needed to understand whether post-transcriptional regulation would be also controlling denitrification-associated protein synthesis in Accumulibacter.

bioRxiv preprint doi: https://doi.org/10.1101/386516; this version posted August 7, 2018. The copyright holder for this preprint (which was not certified by peer review) is the author/funder, who has granted bioRxiv a license to display the preprint in perpetuity. It is made available under aCC-BY-NC-ND 4.0 International license.

Changes in the expression of terminal oxidases in UW-LDO-IC were also identified. All subunits of the terminal cytochrome c oxidase aa_3 were upregulated during the entire micro-aerobic phase (Fig. 5A), indicating active aerobic respiration by this microorganism. Transcriptomic results also showed that the cbb_3-type cytochrome oxidase transcripts decreased when DO increased in the reactor (Fig. 5B). Changes in cytochrome ba_3 oxidase transcript levels were less pronounced than those observed in the other terminal oxidases (maximum $\Delta\log_2$(RPKM) read count < 0.5) (Fig. 5C), likely indicating a minor role of this enzyme during redox condition variations.

We compared the expression of these genes during high and low oxygen concentrations using data from reference (46) (Fig. 4). In both cases, the transcriptional expression of the low-affinity aa_3 cytochrome oxidase increased during the aerobic stage and remained upregulated until the cycle end (Fig. 4D). On the other side, cbb_3-type cytochrome oxidase transcript abundance drastically decreased after turning on aeration in the high-aerated system, whereas the same gene in UW-LDO-IC remained upregulated during the first hour of minimal aeration, corroborating its function as a terminal oxidase induced by limited-oxygen conditions (Fig. 4E). Unlike UW-LDO-IC, Accumulibacter UW-1 had high ba_3 cytochrome c oxidase expression during the anaerobic stages, which declined after aeration started (Fig. 4F). Differences in the expression profile of the latter cytochrome suggests differential gene expression control among these two clades.

Overall, these results demonstrated how expression patterns of the genes responsible for denitrification and aerobic respiration, specifically *nar*, *nir* and *cbb3*, showed upregulation during the beginning of the micro-aerobic stage, supporting our hypothesis that Accumulibacter

bioRxiv preprint doi: https://doi.org/10.1101/386516; this version posted August 7, 2018. The copyright holder for this preprint (which was not certified by peer review) is the author/funder, who has granted bioRxiv a license to display the preprint in perpetuity. It is made available under aCC-BY-NC-ND 4.0 International license.

552 UW-LDO-IC is a denitrifying microorganism capable of simultaneously respiring oxygen and
553 nitrate under micro-aerobic conditions.

554 **Validation of RNA-seq with RT-qPCR**

555 RT-qPCR was conducted on six genes related to anoxic and aerobic respiration (*narG, nirS-*
556 *1, norZ, nosZ, ccoN and ctaD*) to validate RNA sequencing results (Fig. 6). The no-reverse
557 transcription control (NRTC) was used to evaluate the background caused by trace DNA
558 contamination. The average of the difference in Ct (threshold cycle) values between the cDNA
559 and NRTC control was 10 cycles, indicating that DNA contamination was negligible. The copy
560 number of the RNA polymerase sigma-54 factor, encoded by the *rpoN* gene, was used as a
561 reference gene for normalization of the RT-qPCR data, since this gene showed no significant
562 changes (ΔRPKM < 1) in the RNA sequencing results and has been previously used as a
563 reference gene for qPCR normalization in other bacteria (72). The RT-qPCR transcriptomic
564 profile in Fig. 6 was obtained by normalizing each point by the minimum number of copies
565 across the cycle. In all cases, genes regulation trends identified by RT-qPCR agree with those by
566 RNA sequencing (Fig. 6), considering a Pearson correlation coefficient > 0.5, except for *norZ*,
567 where no significant changes in the expression of this gene was quantified (fold-change < 2).

568 **FNR-type regulator controlling denitrification and aerobic respiration in**
569 **Accumulibacter.**

570
571 To identify putative regulatory mechanisms of Accumulibacter's respiratory machinery, an
572 upstream motif analysis was conducted. A sequence motif was identified in the intergenic
573 regions upstream of genes with similar expression patterns: *nar, nir, nos* and cbb_3 operons of
574 Accumulibacter UW-LDO-IC (Fig. 7A). Comparison of this motif with the Prokaryote DNA

bioRxiv preprint doi: https://doi.org/10.1101/386516; this version posted August 7, 2018. The copyright holder for this preprint (which was not certified by peer review) is the author/funder, who has granted bioRxiv a license to display the preprint in perpetuity. It is made available under aCC-BY-NC-ND 4.0 International license.

motif database, using the scanning algorithm Tomtom (73) (p-value = 3.04e-08), classified this sequence as the binding site of FNR, a relatively well-studied member of the CRP/FNR family of transcriptional regulators previously characterized in other proteobacteria (74). FNR is a global regulator of the anaerobic metabolism, reported to be necessary for expression of denitrification and aerobic respiratory pathways (75) and its activity is directly inhibited by oxygen via destruction of a labile iron-sulfur cluster (76).

Subsequent homology searches of this motif sequence were performed in the intergenic region of other genomes of Accumulibacter (p-values < 1e-05). The computational analysis predicted this motif to be located upstream of 165 different genes/operons across all genomes. According to the KEGG category III classification, the majority of these genes appear to be part of metabolic processes involved in carbohydrate and energy metabolism (Fig. 7B). Fig. 7C lists genes with an FNR motif present in at least four Accumulibacter genomes. According to this analysis, FNR auto regulates its own expression, the transcription of genes involved in (a) denitrification, (b) aerobic respiration, including the aa_3 and ba_3 cytochrome oxidases operons, (c) the biosynthesis of tetrapyrrole heme rings, a prosthetic group of many proteins involved in respiration and the metabolism and transport of oxygen (77), and (c) cytochromes c2 and c4, which are electron donors for aa_3 and cbb_3 oxidases (78, 79).

Furthermore, FNR seems to participate in the regulation of carbon uptake, since in many cases, its binding site was positioned upstream of a phosphate acetyltransferase (*pta*) (Fig. 7C). Previously, another palindromic sequence was identified upstream of this gene and postulated this motif as the transcriptional factor PhaR binding site (46). Our findings point to another regulatory mechanism for carbon uptake, relying on oxygen availability. In *Escherichia coli*, chromatin immunoprecipitation sequencing (ChIP-seq) tests revealed a putative binding site for

bioRxiv preprint doi: https://doi.org/10.1101/386516; this version posted August 7, 2018. The copyright holder for this preprint (which was not certified by peer review) is the author/funder, who has granted bioRxiv a license to display the preprint in perpetuity. It is made available under aCC-BY-NC-ND 4.0 International license.

598 FNR upstream of the *pta* operon (80) and RT-qPCR experiments in *fnr* mutants demonstrated
599 that this regulator has a positive effect on the operon transcription (81). Although the FNR
600 binding site was also located upstream of polyhydroxyalkanoic acid (PHA) synthase (*phaC*) in
601 multiple genomes of Accumulibacter, S. M. He and K. D. McMahon (69) did not observe
602 changes in the transcript abundance of *phaC* after exposure to oxygen and, to our knowledge,
603 FNR regulation has not been connected to PHA synthesis in other studied organisms. However,
604 since regulation may vary among Accumulibacter clades, further experiments still need to be
605 carried out to evaluate the effect of oxygen on PHA accumulation in Accumulibacter.
606 Furthermore, in a few Accumulibacter genomes, the FNR motif was also found upstream of
607 genes involved in glycolysis/gluconeogenesis (pyruvate dehydrogenase E1 component (*aceE),*
608 phosphoenolpyruvate carboxykinase (*pepck*) and pyruvate kinase (*pkm*)), which may indicate
609 evolution of this pathway towards an oxygen-independent mechanism. Overall, these results
610 provide evidence for oxygen-driven gene expression regulation, not only as an important factor
611 in the adaptation of Accumulibacter's metabolism to low-DO and anoxic conditions, but also in
612 that oxygen concentration may directly influence Accumulibacter's ability to metabolize carbon.

613 The transcriptional pattern of genes with putative FNR binding sites in UW-LDO-IC were
614 analyzed for O_2-dependant changes in transcript abundance. The expression profile of 25
615 operons were grouped by similarity (Pearson correlation), resulting in 6 clusters with different
616 transcriptional patterns regulated in an oxygen-dependent manner (Fig. 8). Three of these
617 clusters were associated with positive control by FNR, since they showed increase in transcript
618 abundance during early anaerobic (Cluster A), late anaerobic (Cluster B) and early micro-aerobic
619 (Cluster C) stages. These three clusters included genes implicated in denitrification (*nar, nir* and
620 *nos* operons), micro-aerobic respiration (*cco* operon and *hemN*), electron transport (cytochrome

bioRxiv preprint doi: https://doi.org/10.1101/386516; this version posted August 7, 2018. The copyright holder for this preprint (which was not certified by peer review) is the author/funder, who has granted bioRxiv a license to display the preprint in perpetuity. It is made available under aCC-BY-NC-ND 4.0 International license.

c2 and c4), response to stress (*uspA*), oxygen detection (hemerythrin) and acetate-uptake (*pta*). On the contrary, Clusters C, D and E showed negative regulation by FNR (Fig. 8). The unique transcriptional profile of the transcriptional regulator FNR (Cluster C) might be attributed to the effect of negative autoregulation that FNR has on its own transcription during anaerobic conditions (82). Finally, Clusters D and E were induced during the aerobic stage, with Cluster D comprising genes induced during the entire aerobic stage, and Cluster E genes with higher expression at the end of the cycle (Fig. 8). The machinery for aerobic respiration under high-oxygen conditions was enclosed by Cluster E, including the low-O_2 affinity cytochromes aa_3 and ba_3 oxidases and a protein involved in the synthesis of heme A, a prosthetic group required by cytochrome a-type respiratory oxidases. Interestingly, the first subunit of the ba_3 oxidase enzyme was not identified as part of this operon, which may explain the differences observed in the expression levels (Fig. 5C). A second copy of the nitrite reductase enzyme (*nirS-2*) also clustered within this group displaying higher transcript abundance during the aerobic stage. Differences in the regulatory mechanisms of these homologs might be a consequence of gene acquisition from different systems.

The existence of different expression patterns in genes putatively regulated by FNR, indicates that its transcription could be affected by additional regulatory mechanisms, such as combinatorial binding of other regulators and/or epigenetic signals (83). Other transcriptional factors identified in the Accumulibacter genomes, including NreABC, NsrR, NorR and RegAB, might also serve as signals of none or low-oxygen concentration and regulate part of the anoxic and aerobic respiratory pathways, as it has been described in other microorganisms (84-87). However, at the time, no other binding site associated to one of these regulatory elements has been identified in Accumulibacter.

bioRxiv preprint doi: https://doi.org/10.1101/386516; this version posted August 7, 2018. The copyright holder for this preprint (which was not certified by peer review) is the author/funder, who has granted bioRxiv a license to display the preprint in perpetuity. It is made available under aCC-BY-NC-ND 4.0 International license.

644 Overall, this study dissects the metabolic response of Accumulibacter to oxygen-limited
645 conditions. The comparative genomic results provide evidence for the unique respiratory
646 machinery encoded in the newly assembled genome, Accumulibacter UW-LDO-IC, which
647 confers this strain the capability to simultaneously reduce oxygen and nitrogenous compounds.
648 Simultaneous upregulation of both aerobic and anoxic respiratory pathways and co-regulation by
649 the FNR transcriptional factor further support the use of multiple electron acceptors by UW-
650 LDO-IC. Further studies should include experiments analyzing the transcriptional regulation of
651 these pathways at a genome-scale level, using modern approaches such as transcriptional
652 regulatory networks (TRN) and genome wide binding site-locations methods, like ChIP-seq (88)
653 and DNA affinity purification (DAP)- sequencing (89).

654 **ACKNOWLEDGMENTS**

655 This work was partially supported by funding from the National Science Foundation (CBET-
656 1435661, CBET-1803055 and MCB-1518130), the UW-Madison Office of the Vice Chancellor
657 for Research and Graduate Education, and the Madison Metropolitan Sewerage District.
658 Additional funding from the Chilean National Commission for Scientific and Technological
659 Research (CONICYT) as a fellowship to Pamela Camejo is also acknowledged. The work
660 conducted by the U.S. Department of Energy Joint Genome Institute, a DOE Office of Science
661 User Facility, is supported by the Office of Science of the U.S. Department of Energy under
662 Contract No. DE-AC02-05CH11231. Any opinions expressed in this paper are those of the
663 authors and do not necessarily reflect the views of the agency; therefore, no official endorsement
664 should be inferred. Any mention of trade names or commercial products does not constitute
665 endorsement or recommendation for use.

666 **FIGURES**

bioRxiv preprint doi: https://doi.org/10.1101/386516; this version posted August 7, 2018. The copyright holder for this preprint (which was not certified by peer review) is the author/funder, who has granted bioRxiv a license to display the preprint in perpetuity. It is made available under aCC-BY-NC-ND 4.0 International license.

Figure 1. Nutrient profile of phosphorus, acetate, nitrogenous compounds and oxygen concentration in the lab-scale SBR on day-522. Dotted lines separate anaerobic (ANA), micro-aerobic (AER) and settling (SET) periods. Red bars indicate time-points used for RNA-seq (letters in red corresponds to samples names). The period of Media A (acetate and phosphate containing) and Media B (ammonia containing) addition are indicated for the anaerobic stage.

Figure 2. Phylogeny of Accumulibacter UW-LDO-IC. (A) Neighbor-joining phylogenetic tree based on nucleic acid sequences of *ppk1* found in Accumulibacter genomes. (B) RAxML phylogenetic tree of a concatenated alignment of 38 marker genes (nucleotide sequences) of the Accumulibacter genus. Bootstrap values are shown in the tree branches based on 1000 and 100 bootstrap replicates, respectively. The scale bar represents the number of nucleotide substitutions per site.

Figure 3. Gene expression profile patterns of denitrifying-related genes. Relative transcript abundances of (A) nitrate, (B) nitrite, (C) nitric oxide and (D) nitrous oxide reductase genes, and (E) nitrite/nitrate transporters in Accumulibacter UW-LDO-IC during the anaerobic (white panel) and micro-aerobic (grey panel) phases. Each time point's expression value was normalized to the minimum expression of each gene over the cycle.

Figure 4. Gene expression comparison among Clade IC and IIA. Normalized transcript abundance of denitrification-related genes: (A) *nirS*, (B) *norZ* and (C) *nosZ;* and aerobic respiration-related genes: (D) aa_3 cytochrome subunit I , (E) cbb_3 subunit ccoN and (F) ba_3 subunit *cbaA* of Accumulibacter UW-TNR-IC (solid line) and UW-1 (dotted line) (46) during the aerobic stage of an EBPR cycle.

Figure 5. Gene expression profile patterns of aerobic respiration-related genes. Relative transcripts abundance of (A) aa_3, (B) cbb_3 and (C) ba_3 cytochrome c oxidases in Accumulibacter

bioRxiv preprint doi: https://doi.org/10.1101/386516; this version posted August 7, 2018. The copyright holder for this preprint (which was not certified by peer review) is the author/funder, who has granted bioRxiv a license to display the preprint in perpetuity. It is made available under aCC-BY-NC-ND 4.0 International license.

690 UW-TNR-IC during the anaerobic (white panel) and micro-aerobic (grey panel) phases. Each
691 time point's expression value was normalized to the minimum expression of each gene over the
692 cycle.

693 **Figure 6.** Comparison of the transcriptomic profiles obtained from RT-qPCR (gene copies
694 normalized by *rpoN* copies, solid black lines) and RNA sequencing (ΔLog_2 RPKM, dotted red
695 lines). Expression of genes involved in denitrification, *narG*, *nirS*, *norZ* and *nosZ*, are presented
696 in panels A-D. Genes involved in aerobic respiration, *ccoN* (*cbb*$_3$) and *ctaD* (*aa*$_3$) are included in
697 panels E-F.

698 **Figure 7. The FNR regulon in Accumulibacter.** (A) Motif diagram showing a putative
699 FNR-binding site identified upstream of respiratory genes. (B) Distribution of KEGG functional
700 categories in the fraction of genes with the FNR motif in genomes of Accumulibacter. (C) The
701 predicted conservation of the FNR regulon determined in the Accumulibacter lineage; only genes
702 with motifs present in at least 4 genomes are shown. Black indicates that the corresponding strain
703 does not possess the corresponding gene, blue indicates that the strain possesses the gene, but an
704 FNR-motif was not located within the upstream intergenic region. Yellow indicates that the gene
705 with an FNR-motif is present in the genome.

706 **Figure 8. Transcription profile heatmap of members of the FNR regulon in UW-LDO-**
707 **IC**. The colors represent the relative level of mRNA abundance at each time point of the cycle
708 compared to the mean level of expression (yellow=high expression, dark blue=low expression).
709 Genes were clustered according to their expression profiles. Lateral grey bars indicate genes
710 belonging to the same operon. Group A and B contain genes whose expression levels negatively
711 correlate with oxygen tension (positively regulated by FNR). Group C, D and E contains genes

bioRxiv preprint doi: https://doi.org/10.1101/386516; this version posted August 7, 2018. The copyright holder for this preprint (which was not certified by peer review) is the author/funder, who has granted bioRxiv a license to display the preprint in perpetuity. It is made available under aCC-BY-NC-ND 4.0 International license.

upregulated during high oxygen levels (negatively regulated by FNR). ANA: anaerobic, AER: micro-aerobic.

REFERENCES

1. Mielczarek AT, Nguyen HT, Nielsen JL, Nielsen PH. 2013. Population dynamics of bacteria involved in enhanced biological phosphorus removal in Danish wastewater treatment plants. Water Res 47:1529-44.
2. Lemaire R, Yuan Z, Blackall LL, Crocetti GR. 2008. Microbial distribution of Accumulibacter spp. and Competibacter spp. in aerobic granules from a lab-scale biological nutrient removal system. Environ Microbiol 10:354-63.
3. Wang X, Wang S, Xue T, Li B, Dai X, Peng Y. 2015. Treating low carbon/nitrogen (C/N) wastewater in simultaneous nitrification-endogenous denitrification and phosphorous removal (SNDPR) systems by strengthening anaerobic intracellular carbon storage. Water Res 77:191-200.
4. Yilmaz G, Lemaire R, Keller J, Yuan Z. 2008. Simultaneous nitrification, denitrification, and phosphorus removal from nutrient-rich industrial wastewater using granular sludge. Biotechnol Bioeng 100:529-41.
5. Mino T, Van Loosdrecht MCM, Heijnen JJ. 1998. Microbiology and biochemistry of the enhanced biological phosphate removal process. Water Research 32:3193-3207.
6. He S, Gall DL, McMahon KD. 2007. "Candidatus accumulibacter" population structure in enhanced biological phosphorus removal Sludges as revealed by polyphosphate kinase genes. Applied and Environmental Microbiology 73:5865-5874.

bioRxiv preprint doi: https://doi.org/10.1101/386516; this version posted August 7, 2018. The copyright holder for this preprint (which was not certified by peer review) is the author/funder, who has granted bioRxiv a license to display the preprint in perpetuity. It is made available under aCC-BY-NC-ND 4.0 International license.

7. Peterson SB, Warnecke F, Madejska J, McMahon KD, Hugenholtz P. 2008. Environmental distribution and population biology of Candidatus Accumulibacter, a primary agent of biological phosphorus removal. Environmental Microbiology 10:2692-2703.

8. Camejo PY, Owen BR, Martirano J, Ma J, Kapoor V, Santo Domingo J, McMahon KD, Noguera DR. 2016. Candidatus Accumulibacter phosphatis clades enriched under cyclic anaerobic and microaerobic conditions simultaneously use different electron acceptors. Water Research 102:125-137.

9. Mao Y, Graham DW, Tamaki H, Zhang T. 2015. Dominant and novel clades of Candidatus Accumulibacter phosphatis in 18 globally distributed full-scale wastewater treatment plants. Sci Rep 5:11857.

10. Flowers JJ, He S, Yilmaz S, Noguera DR, McMahon KD. 2009. Denitrification capabilities of two biological phosphorus removal sludges dominated by different "Candidatus Accumulibacter" clades. Environ Microbiol Rep 1:583-588.

11. Kim JM, Lee HJ, Lee DS, Jeon CO. 2013. Characterization of the Denitrification-Associated Phosphorus Uptake Properties of "Candidatus Accumulibacter phosphatis" Clades in Sludge Subjected to Enhanced Biological Phosphorus Removal. Applied and Environmental Microbiology 79:1969-1979.

12. Welles L, Tian WD, Saad S, Abbas B, Lopez-Vazquez CM, Hooijmans CM, van Loosdrecht MC, Brdjanovic D. 2015. Accumulibacter clades Type I and II performing kinetically different glycogen-accumulating organisms metabolisms for anaerobic substrate uptake. Water Res 83:354-66.

bioRxiv preprint doi: https://doi.org/10.1101/386516; this version posted August 7, 2018. The copyright holder for this preprint (which was not certified by peer review) is the author/funder, who has granted bioRxiv a license to display the preprint in perpetuity. It is made available under aCC-BY-NC-ND 4.0 International license.

13. Slater FR, Johnson CR, Blackall LL, Beiko RG, Bond PL. 2010. Monitoring associations between clade-level variation, overall community structure and ecosystem function in enhanced biological phosphorus removal (EBPR) systems using terminal-restriction fragment length polymorphism (T-RFLP). Water Research 44:4908-4923.

14. Cokro AA, Law Y, Williams RBH, Cao Y, Nielsen PH, Wuertz S. 2017. Non-denitrifying polyphosphate accumulating organisms obviate requirement for anaerobic condition. Water Research 111:393-403.

15. Carvalho G, Lemos PC, Oehmen A, Reis MAM. 2007. Denitrifying phosphorus removal: Linking the process performance with the microbial community structure. Water Research 41:4383-4396.

16. Oehmen A, Carvalho G, Lopez-Vazquez CM, van Loosdrecht MCM, Reis MAM. 2010. Incorporating microbial ecology into the metabolic modelling of polyphosphate accumulating organisms and glycogen accumulating organisms. Water Research 44:4992-5004.

17. Lanham AB, Moita R, Lemos PC, Reis MA. 2011. Long-term operation of a reactor enriched in Accumulibacter clade I DPAOs: performance with nitrate, nitrite and oxygen. Water Sci Technol 63:352-9.

18. Saad SA, Welles L, Abbas B, Lopez-Vazquez CM, van Loosdrecht MCM, Brdjanovic D. 2016. Denitrification of nitrate and nitrite by 'Candidatus Accumulibacter phosphatis' clade IC. Water Research 105:97-109.

19. Rubio-Rincon FJ, Lopez-Vazquez CM, Welles L, van Loosdrecht MCM, Brdjanovic D. 2017. Cooperation between Candidatus Competibacter and Candidatus Accumulibacter clade I, in denitrification and phosphate removal processes. Water Research 120:156-164.

bioRxiv preprint doi: https://doi.org/10.1101/386516; this version posted August 7, 2018. The copyright holder for this preprint (which was not certified by peer review) is the author/funder, who has granted bioRxiv a license to display the preprint in perpetuity. It is made available under aCC-BY-NC-ND 4.0 International license.

781 20. Zilles JL, Peccia J, Kim MW, Hung CH, Noguera DR. 2002. Involvement of
782 Rhodocyclus-related organisms in phosphorus removal in full-scale wastewater treatment
783 plants. Applied and Environmental Microbiology 68:2763-2769.
784 21. Park HD, Whang LM, Reusser SR, Noguera DR. 2006. Taking advantage of aerated-
785 anoxic operation in a full-scale University of Cape Town process. Water Environment
786 Research 78:637-642.
787 22. APHA. Standard methods for the examination of water and wastewater, p. *In* Andrew D.
788 Eaton LSC, Eugene W. Rice, Arnold E. Greenberg (ed),
789 23. Caporaso JG, Lauber CL, Walters WA, Berg-Lyons D, Lozupone CA, Turnbaugh PJ,
790 Fierer N, Knight R. 2011. Global patterns of 16S rRNA diversity at a depth of millions of
791 sequences per sample. Proceedings of the National Academy of Sciences of the United
792 States of America 108:4516-4522.
793 24. Caporaso JG, Kuczynski J, Stombaugh J, Bittinger K, Bushman FD, Costello EK, Fierer
794 N, Pena AG, Goodrich JK, Gordon JI, Huttley GA, Kelley ST, Knights D, Koenig JE,
795 Ley RE, Lozupone CA, McDonald D, Muegge BD, Pirrung M, Reeder J, Sevinsky JR,
796 Tumbaugh PJ, Walters WA, Widmann J, Yatsunenko T, Zaneveld J, Knight R. 2010.
797 QIIME allows analysis of high-throughput community sequencing data. Nature Methods
798 7:335-336.
799 25. Edgar RC, Haas BJ, Clemente JC, Quince C, Knight R. 2011. UCHIME improves
800 sensitivity and speed of chimera detection. Bioinformatics 27:2194-200.
801 26. Mielczarek AT, Saunders AM, Larsen P, Albertsen M, Stevenson M, Nielsen JL, Nielsen
802 PH. 2013. The Microbial Database for Danish wastewater treatment plants with nutrient

bioRxiv preprint doi: https://doi.org/10.1101/386516; this version posted August 7, 2018. The copyright holder for this preprint (which was not certified by peer review) is the author/funder, who has granted bioRxiv a license to display the preprint in perpetuity. It is made available under aCC-BY-NC-ND 4.0 International license.

803 removal (MiDas-DK) - a tool for understanding activated sludge population dynamics
804 and community stability. Water Science and Technology 67:2519-2526.
805 27. Nurk S, Meleshko D, Korobeynikov A, Pevzner PA. 2017. metaSPAdes: a new versatile
806 metagenomic assembler. Genome Res 27:824-834.
807 28. Wu YW, Tang YH, Tringe SG, Simmons BA, Singer SW. 2014. MaxBin: an automated
808 binning method to recover individual genomes from metagenomes using an expectation-
809 maximization algorithm. Microbiome 2.
810 29. Parks DH, Imelfort M, Skennerton CT, Hugenholtz P, Tyson GW. 2015. CheckM:
811 assessing the quality of microbial genomes recovered from isolates, single cells, and
812 metagenomes. Genome Res 25:1043-55.
813 30. Darling AE, Jospin G, Lowe E, Matsen FAt, Bik HM, Eisen JA. 2014. PhyloSift:
814 phylogenetic analysis of genomes and metagenomes. PeerJ 2:e243.
815 31. Eren AM, Esen OC, Quince C, Vineis JH, Morrison HG, Sogin ML, Delmont TO. 2015.
816 Anvi'o: an advanced analysis and visualization platform for 'omics data. PeerJ 3:e1319.
817 32. Warren RL, Yang C, Vandervalk BP, Behsaz B, Lagman A, Jones SJM, Birol I. 2015.
818 LINKS: Scalable, alignment-free scaffolding of draft genomes with long reads.
819 Gigascience 4.
820 33. Hanson NW, Konwar KM, Hawley AK, Altman T, Karp PD, Hallam SJ. 2014. Metabolic
821 pathways for the whole community. BMC Genomics 15:619.
822 34. Richter M, Rossello-Mora R. 2009. Shifting the genomic gold standard for the
823 prokaryotic species definition. Proceedings of the National Academy of Sciences of the
824 United States of America 106:19126-19131.

bioRxiv preprint doi: https://doi.org/10.1101/386516; this version posted August 7, 2018. The copyright holder for this preprint (which was not certified by peer review) is the author/funder, who has granted bioRxiv a license to display the preprint in perpetuity. It is made available under aCC-BY-NC-ND 4.0 International license.

825 35. Stamatakis A. 2006. RAxML-VI-HPC: maximum likelihood-based phylogenetic analyses
826 with thousands of taxa and mixed models. Bioinformatics 22:2688-90.
827 36. Clark K, Karsch-Mizrachi I, Lipman DJ, Ostell J, Sayers EW. 2016. GenBank. Nucleic
828 Acids Research 44:D67-D72.
829 37. Wright ES. 2015. DECIPHER: harnessing local sequence context to improve protein
830 multiple sequence alignment. Bmc Bioinformatics 16.
831 38. Magoc T, Salzberg SL. 2011. FLASH: fast length adjustment of short reads to improve
832 genome assemblies. Bioinformatics 27:2957-2963.
833 39. Kopylova E, Noe L, Touzet H. 2012. SortMeRNA: fast and accurate filtering of
834 ribosomal RNAs in metatranscriptomic data. Bioinformatics 28:3211-3217.
835 40. Bushnell B. 2014. BBMap: A Fast, Accurate, Splice-Aware Aligner. Ernest Orlando
836 Lawrence Berkeley National Laboratory, Berkeley, CA.
837 41. Anders S, Pyl PT, Huber W. 2015. HTSeq-a Python framework to work with high-
838 throughput sequencing data. Bioinformatics 31:166-169.
839 42. Mortazavi A, Williams BA, Mccue K, Schaeffer L, Wold B. 2008. Mapping and
840 quantifying mammalian transcriptomes by RNA-Seq. Nature Methods 5:621-628.
841 43. Wright ES, Yilmaz LS, Ram S, Gasser JM, Harrington GW, Noguera DR. 2014.
842 Exploiting extension bias in polymerase chain reaction to improve primer specificity in
843 ensembles of nearly identical DNA templates. Environmental Microbiology 16:1354-
844 1365.
845 44. Bailey TL, Williams N, Misleh C, Li WW. 2006. MEME: discovering and analyzing
846 DNA and protein sequence motifs. Nucleic Acids Res 34:W369-73.

bioRxiv preprint doi: https://doi.org/10.1101/386516; this version posted August 7, 2018. The copyright holder for this preprint (which was not certified by peer review) is the author/funder, who has granted bioRxiv a license to display the preprint in perpetuity. It is made available under aCC-BY-NC-ND 4.0 International license.

847 45. Grant CE, Bailey TL, Noble WS. 2011. FIMO: scanning for occurrences of a given
848 motif. Bioinformatics 27:1017-8.
849 46. Oyserman BO, Noguera DR, del Rio TG, Tringe SG, McMahon KD. 2016.
850 Metatranscriptomic insights on gene expression and regulatory controls in Candidatus
851 Accumulibacter phosphatis. Isme Journal 10:810-822.
852 47. Barr JJ, Dutilh BE, Skennerton CT, Fukushima T, Hastie ML, Gorman JJ, Tyson GW,
853 Bond PL. 2016. Metagenomic and metaproteomic analyses of Accumulibacter
854 phosphatis-enriched floccular and granular biofilm. Environ Microbiol 18:273-87.
855 48. Mao Y, Yu K, Xia Y, Chao Y, Zhang T. 2014. Genome reconstruction and gene
856 expression of "Candidatus Accumulibacter phosphatis" Clade IB performing biological
857 phosphorus removal. Environ Sci Technol 48:10363-71.
858 49. Skennerton CT, Barr JJ, Slater FR, Bond PL, Tyson GW. 2015. Expanding our view of
859 genomic diversity in Candidatus Accumulibacter clades. Environmental Microbiology
860 17:1574-1585.
861 50. Flowers JJ, He SM, Malfatti S, del Rio TG, Tringe SG, Hugenholtz P, McMahon KD.
862 2013. Comparative genomics of two 'Candidatus Accumulibacter' clades performing
863 biological phosphorus removal. Isme Journal 7:2301-2314.
864 51. Wu DY, Jospin G, Eisen JA. 2013. Systematic Identification of Gene Families for Use as
865 "Markers" for Phylogenetic and Phylogeny-Driven Ecological Studies of Bacteria and
866 Archaea and Their Major Subgroups. Plos One 8:e77033.
867 52. Parks DH, Rinke C, Chuvochina M, Chaumeil PA, Woodcroft BJ, Evans PN, Hugenholtz
868 P, Tyson GW. 2017. Recovery of nearly 8,000 metagenome-assembled genomes
869 substantially expands the tree of life. Nature Microbiology 2:1533-1542.

bioRxiv preprint doi: https://doi.org/10.1101/386516; this version posted August 7, 2018. The copyright holder for this preprint (which was not certified by peer review) is the author/funder, who has granted bioRxiv a license to display the preprint in perpetuity. It is made available under aCC-BY-NC-ND 4.0 International license.

870 53. Konstantinidis KT, Tiedje JM. 2005. Genomic insights that advance the species
871 definition for prokaryotes. Proceedings of the National Academy of Sciences of the
872 United States of America 102:2567-2572.
873 54. Varghese NJ, Mukherjee S, Ivanova N, Konstantinidis KT, Mavrommatis K, Kyrpides
874 NC, Pati A. 2015. Microbial species delineation using whole genome sequences. Nucleic
875 Acids Res 43:6761-71.
876 55. Oyserman BO, Moya F, Lawson CE, Garcia AL, Vogt M, Heffernen M, Noguera DR,
877 McMahon KD. 2016. Ancestral genome reconstruction identifies the evolutionary basis
878 for trait acquisition in polyphosphate accumulating bacteria. ISME J 10:2931-2945.
879 56. Sparacino-Watkins C, Stolz JF, Basu P. 2014. Nitrate and periplasmic nitrate reductases.
880 Chem Soc Rev 43:676-706.
881 57. Ahn J, Daidou T, Tsuneda S, Hirata A. 2001. Metabolic behavior of denitrifying
882 phosphate-accumulating organisms under nitrate and nitrite electron acceptor conditions.
883 J Biosci Bioeng 92:442-6.
884 58. Richardson DJ. 2000. Bacterial respiration: a flexible process for a changing
885 environment. Microbiology 146 (Pt 3):551-71.
886 59. Flory JE, Donohue TJ. 1997. Transcriptional control of several aerobically induced
887 cytochrome structural genes in Rhodobacter sphaeroides. Microbiology-Sgm 143:3101-
888 3110.
889 60. Winstedt L, von Wachenfeldt C. 2000. Terminal oxidases of Bacillus subtilis strain 168:
890 one quinol oxidase, cytochrome aa(3) or cytochrome bd, is required for aerobic growth. J
891 Bacteriol 182:6557-64.

bioRxiv preprint doi: https://doi.org/10.1101/386516; this version posted August 7, 2018. The copyright holder for this preprint (which was not certified by peer review) is the author/funder, who has granted bioRxiv a license to display the preprint in perpetuity. It is made available under aCC-BY-NC-ND 4.0 International license.

892 61. Arai H, Roh JH, Kaplan S. 2008. Transcriptome dynamics during the transition from
893 anaerobic photosynthesis to aerobic respiration in Rhodobacter sphaeroides 2.4.1. J
894 Bacteriol 190:286-99.
895 62. Swem DL, Bauer CE. 2002. Coordination of ubiquinol oxidase and cytochrome cbb(3)
896 oxidase expression by multiple regulators in Rhodobacter capsulatus. J Bacteriol
897 184:2815-20.
898 63. Otten MF, Stork DM, Reijnders WN, Westerhoff HV, Van Spanning RJ. 2001.
899 Regulation of expression of terminal oxidases in Paracoccus denitrificans. Eur J Biochem
900 268:2486-97.
901 64. Mouncey NJ, Kaplan S. 1998. Oxygen regulation of the ccoN gene encoding a
902 component of the cbb3 oxidase in Rhodobacter sphaeroides 2.4.1T: involvement of the
903 FnrL protein. J Bacteriol 180:2228-31.
904 65. Jackson RJ, Elvers KT, Lee LJ, Gidley MD, Wainwright LM, Lightfoot J, Park SF, Poole
905 RK. 2007. Oxygen reactivity of both respiratory oxidases in Campylobacter jejuni: the
906 cydAB genes encode a cyanide-resistant, low-affinity oxidase that is not of the
907 cytochrome bd type. Journal of Bacteriology 189:1604-1615.
908 66. Preisig O, Zufferey R, Thony-Meyer L, Appleby CA, Hennecke H. 1996. A high-affinity
909 cbb3-type cytochrome oxidase terminates the symbiosis-specific respiratory chain of
910 Bradyrhizobium japonicum. J Bacteriol 178:1532-8.
911 67. Keene NA, Reusser SR, Scarborough MJ, Grooms AL, Seib M, Santo Domingo J,
912 Noguera DR. 2017. Pilot plant demonstration of stable and efficient high rate biological
913 nutrient removal with low dissolved oxygen conditions. Water Res 121:72-85.

bioRxiv preprint doi: https://doi.org/10.1101/386516; this version posted August 7, 2018. The copyright holder for this preprint (which was not certified by peer review) is the author/funder, who has granted bioRxiv a license to display the preprint in perpetuity. It is made available under aCC-BY-NC-ND 4.0 International license.

914 68. Soulimane T, Buse G, Bourenkov GP, Bartunik HD, Huber R, Than ME. 2000. Structure
915 and mechanism of the aberrant ba(3)-cytochrome c oxidase from Thermus thermophilus.
916 Embo Journal 19:1766-1776.
917 69. He SM, McMahon KD. 2011. 'Candidatus Accumulibacter' gene expression in response
918 to dynamic EBPR conditions. Isme Journal 5:329-340.
919 70. He SM, Kunin V, Haynes M, Martin HG, Ivanova N, Rohwer F, Hugenholtz P,
920 McMahon KD. 2010. Metatranscriptomic array analysis of 'Candidatus Accumulibacter
921 phosphatis'-enriched enhanced biological phosphorus removal sludge. Environmental
922 Microbiology 12:1205-1217.
923 71. Bueno E, Mesa S, Bedmar EJ, Richardson DJ, Delgado MJ. 2012. Bacterial adaptation of
924 respiration from oxic to microoxic and anoxic conditions: redox control. Antioxid Redox
925 Signal 16:819-52.
926 72. Chang Q, Amemiya T, Liu J, Xu X, Rajendran N, Itoh K. 2009. Identification and
927 validation of suitable reference genes for quantitative expression of xylA and xylE genes
928 in Pseudomonas putida mt-2. J Biosci Bioeng 107:210-4.
929 73. Gupta S, Stamatoyannopoulos JA, Bailey TL, Noble WS. 2007. Quantifying similarity
930 between motifs. Genome Biology 8.
931 74. Korner H, Sofia HJ, Zumft WG. 2003. Phylogeny of the bacterial superfamily of Crp-Fnr
932 transcription regulators: exploiting the metabolic spectrum by controlling alternative gene
933 programs. FEMS Microbiol Rev 27:559-92.
934 75. Arai H, Kodama T, Igarashi Y. 1997. Cascade regulation of the two CRP/FNR-related
935 transcriptional regulators (ANR and DNR) and the denitrification enzymes in
936 Pseudomonas aeruginosa. Mol Microbiol 25:1141-8.

bioRxiv preprint doi: https://doi.org/10.1101/386516; this version posted August 7, 2018. The copyright holder for this preprint (which was not certified by peer review) is the author/funder, who has granted bioRxiv a license to display the preprint in perpetuity. It is made available under aCC-BY-NC-ND 4.0 International license.

937 76. Green J, Crack JC, Thomson AJ, LeBrun NE. 2009. Bacterial sensors of oxygen. Curr
938 Opin Microbiol 12:145-51.
939 77. Rompf A, Hungerer C, Hoffmann T, Lindenmeyer M, Romling U, Gross U, Doss MO,
940 Arai H, Igarashi Y, Jahn D. 1998. Regulation of Pseudomonas aeruginosa hemF and
941 hemN by the dual action of the redox response regulators Anr and Dnr. Mol Microbiol
942 29:985-97.
943 78. Chang HY, Ahn Y, Pace LA, Lin MT, Lin YH, Gennis RB. 2010. The Diheme
944 Cytochrome c(4) from Vibrio cholerae Is a Natural Electron Donor to the Respiratory
945 cbb(3) Oxygen Reductase. Biochemistry 49:7494-7503.
946 79. Daldal F, Mandaci S, Winterstein C, Myllykallio H, Duyck K, Zannoni D. 2001. Mobile
947 cytochrome c2 and membrane-anchored cytochrome cy are both efficient electron donors
948 to the cbb3- and aa3-type cytochrome c oxidases during respiratory growth of
949 Rhodobacter sphaeroides. J Bacteriol 183:2013-24.
950 80. Myers KS, Yan H, Ong IM, Chung D, Liang K, Tran F, Keles S, Landick R, Kiley PJ.
951 2013. Genome-scale analysis of escherichia coli FNR reveals complex features of
952 transcription factor binding. PLoS Genet 9:e1003565.
953 81. Shalel-Levanon S, San KY, Bennett GN. 2005. Effect of ArcA and FNR on the
954 expression of genes related to the oxygen regulation and the glycolysis pathway in
955 Escherichia coli under microaerobic growth conditions. Biotechnol Bioeng 92:147-59.
956 82. Mettert EL, Kiley PJ. 2007. Contributions of [4Fe-4S]-FNR and integration host factor to
957 fnr transcriptional regulation. J Bacteriol 189:3036-43.
958 83. Casadesus J, Low D. 2006. Epigenetic gene regulation in the bacterial world. Microbiol
959 Mol Biol Rev 70:830-56.

bioRxiv preprint doi: https://doi.org/10.1101/386516; this version posted August 7, 2018. The copyright holder for this preprint (which was not certified by peer review) is the author/funder, who has granted bioRxiv a license to display the preprint in perpetuity. It is made available under aCC-BY-NC-ND 4.0 International license.

960 84. Swem LR, Elsen S, Bird TH, Swem DL, Koch HG, Myllykallio H, Daldal F, Bauer CE.
961 2001. The RegB/RegA two-component regulatory system controls synthesis of
962 photosynthesis and respiratory electron transfer components in Rhodobacter capsulatus. J
963 Mol Biol 309:121-38.
964 85. Pohlmann A, Cramm R, Schmelz K, Friedrich B. 2000. A novel NO-responding regulator
965 controls the reduction of nitric oxide in Ralstonia eutropha. Mol Microbiol 38:626-38.
966 86. Beaumont HJ, Lens SI, Reijnders WN, Westerhoff HV, van Spanning RJ. 2004.
967 Expression of nitrite reductase in Nitrosomonas europaea involves NsrR, a novel nitrite-
968 sensitive transcription repressor. Mol Microbiol 54:148-58.
969 87. Nilkens S, Koch-Singenstreu M, Niemann V, Gotz F, Stehle T, Unden G. 2014.
970 Nitrate/oxygen co-sensing by an NreA/NreB sensor complex of Staphylococcus carnosus.
971 Mol Microbiol 91:381-93.
972 88. Johnson DS, Mortazavi A, Myers RM, Wold B. 2007. Genome-wide mapping of in vivo
973 protein-DNA interactions. Science 316:1497-502.
974 89. O'Malley RC, Huang SC, Song L, Lewsey MG, Bartlett A, Nery JR, Galli M, Gallavotti
975 A, Ecker JR. 2016. Cistrome and Epicistrome Features Shape the Regulatory DNA
976 Landscape. Cell 166:1598.
977

Table 1. Inventory of genes associated with denitrification in complete and draft genomes of *Accumulibacter*. Black and white rectangles represent presence and absence of each gene, respectively. Genes present in the assembled Accumulibacter sp. UW-LDO-IC genome are highlighted in red.
ND: Not determined.

		Clade	ND	ND	IIA	IIC					IIF						IA			IB			IC
Category	**Gene**	**Function**	**66-26**	**UBA704**	**UW-1**	**SK-01**	**UBA5574**	**HKU-2**	**SK-02**	**BA-91**	**BA-94**	**UBA2327**	**SK-11**	**UBA6585**	**SK-12**	**UBA2315**	**UBA6658**	**BA-93**	**UW-2**	**HKU-1**	**UBA2783**	**BA-92**	**UW-LDO-IC**
Transport	*narK*	Nitrate/nitrite transporter		■	■	■	■	■	■	■				■	■	■	■	■	■	■	■	■	
Respiratory Nitrate Reduction	*narI*	Respiratory nitrate reductase gamma chain		■		■	■	■	■	■													
	narJ	Respiratory nitrate reductase delta chain		■		■	■	■	■	■													
	narH	Respiratory nitrate reductase beta chain		■		■	■	■	■	■													
	narG	Respiratory nitrate reductase alpha chain		■		■	■	■	■	■													
Periplasmic Nitrate Reduction	*napD*	Periplasmic nitrate reductase chaperone NapD	■		■						■	■		■		■	■	■	■	■	■	■	
	napA	Periplasmic nitrate reductase subunit	■	■	■						■	■		■		■	■	■	■	■	■	■	
	napG	Ferredoxin-type protein NapG	■	■	■							■	■	■	■	■	■	■	■	■	■	■	
	napH	Ferredoxin-type protein NapH	■	■	■							■	■	■	■	■	■	■	■	■	■	■	
	napB	Periplasmic nitrate reductase subunit	■	■	■							■		■	■	■	■	■	■	■	■	■	
Nitrite Reduction	*nirS*	Nitrite reductase	■		■	■	■	■	■	■		■	■	■	■	■	■	■	■	■	■	■	■
	nirM	Cytochrome c551	■	■	■	■	■	■	■	■	■	■	■	■	■	■	■	■	■	■	■	■	■
	nirN	Nitrite reductase associated c-type cytochrome	■		■	■	■	■	■	■	■		■	■	■	■	■	■	■	■	■	■	■
	nirJ	Heme d1 biosynthesis protein	■		■	■	■	■	■	■	■		■	■	■	■	■	■	■	■	■	■	■
	nirC	Cytochrome c55X precursor	■	■	■	■	■	■	■	■		■	■	■	■	■	■	■	■	■	■	■	■
	nirF	Heme d1 biosynthesis protein	■		■	■	■	■	■	■	■	■	■	■	■	■	■	■	■	■	■	■	■
	nirD/nirL	Heme d1 biosynthesis protein	■	■	■	■	■	■	■	■		■	■	■	■	■	■	■	■	■	■	■	■
	nirG	Heme d1 biosynthesis protein	■		■	■	■	■	■	■		■	■	■	■	■	■	■	■	■	■	■	■
	nirH	Heme d1 biosynthesis protein	■		■	■	■	■	■	■		■	■	■	■	■	■	■	■	■	■	■	■
Nitric Oxide Reduction	*norZ*	Nitric oxide reductase, qNOR-like																					■
Nitrous Oxide Reduction	*nosD*	Nitrous oxide reductase maturation protein	■		■						■			■	■	■	■	■	■	■	■	■	■
	nosZ	Nitrous-oxide reductase	■		■							■	■	■	■	■	■	■	■	■	■	■	■
	nosF	Nitrous oxide reductase maturation protein	■		■							■	■	■	■	■	■	■	■	■	■	■	■
	nosL	Nitrous oxide reductase maturation protein	■		■							■	■	■	■	■	■	■	■		■	■	■
	nosY	Nitrous oxide reductase maturation protein	■		■							■	■	■	■	■	■	■	■	■	■	■	■

Table 2. Inventory of genes associated with aerobic respiration in complete and draft genomes of *Accumulibacter*. Black and white rectangles represent presence and absence of each gene, respectively. Genes present in the assembled Accumulibacter sp. UW-LDO-IC genome are highlighted in red.
ND: Not determined

Clade			ND	ND	IIA	IIC					IIF						IA			IB			IC
Category	**Gene**	**Function**	**66-26**	**UBA704**	**UW-1**	**SK-01**	**UBA5574**	**HKU-2**	**SK-02**	**BA-91**	**BA-94**	**UBA2327**	**SK-11**	**UBA6585**	**SK-12**	**UBA2315**	**UBA6658**	**BA-93**	**UW-2**	**HKU-1**	**UBA2783**	**BA-92**	**UW-LDO-IC**
Cytochrome c oxidation (cbb_3)	*ccoN*	Cytochrome c oxidase, cbb3-type, subunit I	■	■	■	■	■	■	■	□	■	■	■	■	■	□	■	■	■	■	■	□	■
	ccoO	Cytochrome c oxidase, cbb3-type, subunit II	■	■	■	■	■	■	■	■	■	■	■	■	■	□	■	■	■	■	■	■	■
	ccoQ	Cytochrome c oxidase, cbb3-type, small subunit I	■	■	■	■	■	■	■	□	■	■	■	■	■	■	■	■	■	■	■	■	■
	ccoP	Cytochrome c oxidase, cbb3-type, subunit III	■	■	■	■	■	■	■	■	■	■	■	■	■	■	■	■	■	■	■	■	■
	ccoG	Type cbb3 cytochrome oxidase biogenesis protein	■	■	■	■	■	■	■	■	■	■	■	■	■	■	■	■	■	■	■	■	■
	ccoH	Cytochrome c oxidase, cbb3-type, small subunit II	■	■	■	■	■	■	■	■	■	■	■	■	■	■	■	■	■	■	■	■	■
	ccoI	Type cbb3 cytochrome oxidase biogenesis protein	■	■	■	■	■	■	■	■	■	□	■	■	■	■	■	■	■	■	■	■	■
	ccoS	Type cbb3 cytochrome oxidase biogenesis protein	■	■	■	■	■	■	■	□	■	□	□	■	■	□	■	■	■	■	■	□	■
Cytochrome c oxidase (ba_3)	*cbaA*	Cytochrome c oxidase (B(O/a)3-type) chain I	□	□	■	■	■	□	■	□	■	■	■	■	■	■	■	■	■	■	■	■	■
	cbaB	Cytochrome c oxidase (B(O/a)3-type) chain II	□	□	■	■	■	□	■	■	■	■	■	■	■	■	■	■	■	■	■	■	■
Cytochrome c oxidase (aa_3)	*ctaD*	Cytochrome c oxidase polypeptide I	■	■	■	■	□	■	■	■	□	□	□	□	□	□	■	■	■	□	□	■	■
	ctaC	Cytochrome c oxidase polypeptide II	■	■	■	■	■	■	■	■	□	■	■	■	■	■	■	■	■	■	■	■	■
	ctaE	Cytochrome c oxidase polypeptide III	■	■	■	■	■	■	■	■	■	■	■	■	■	■	■	■	■	■	■	■	■

bioRxiv preprint doi: https://doi.org/10.1101/386516; this version posted August 7, 2018. The copyright holder for this preprint (which was not certified by peer review) is the author/funder, who has granted bioRxiv a license to display the preprint in perpetuity. It is made available under CC BY-NC-ND 4.0 International license.

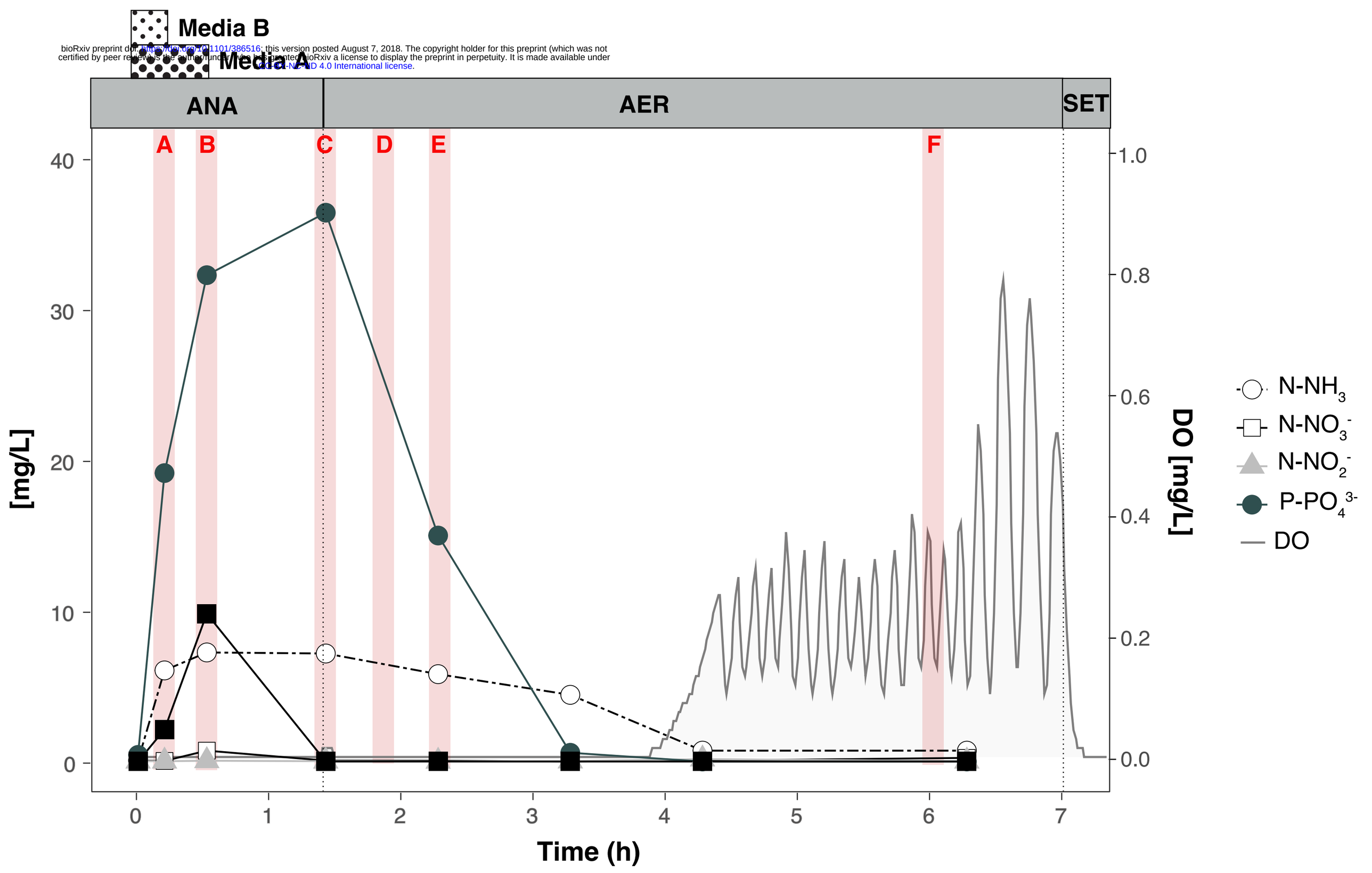

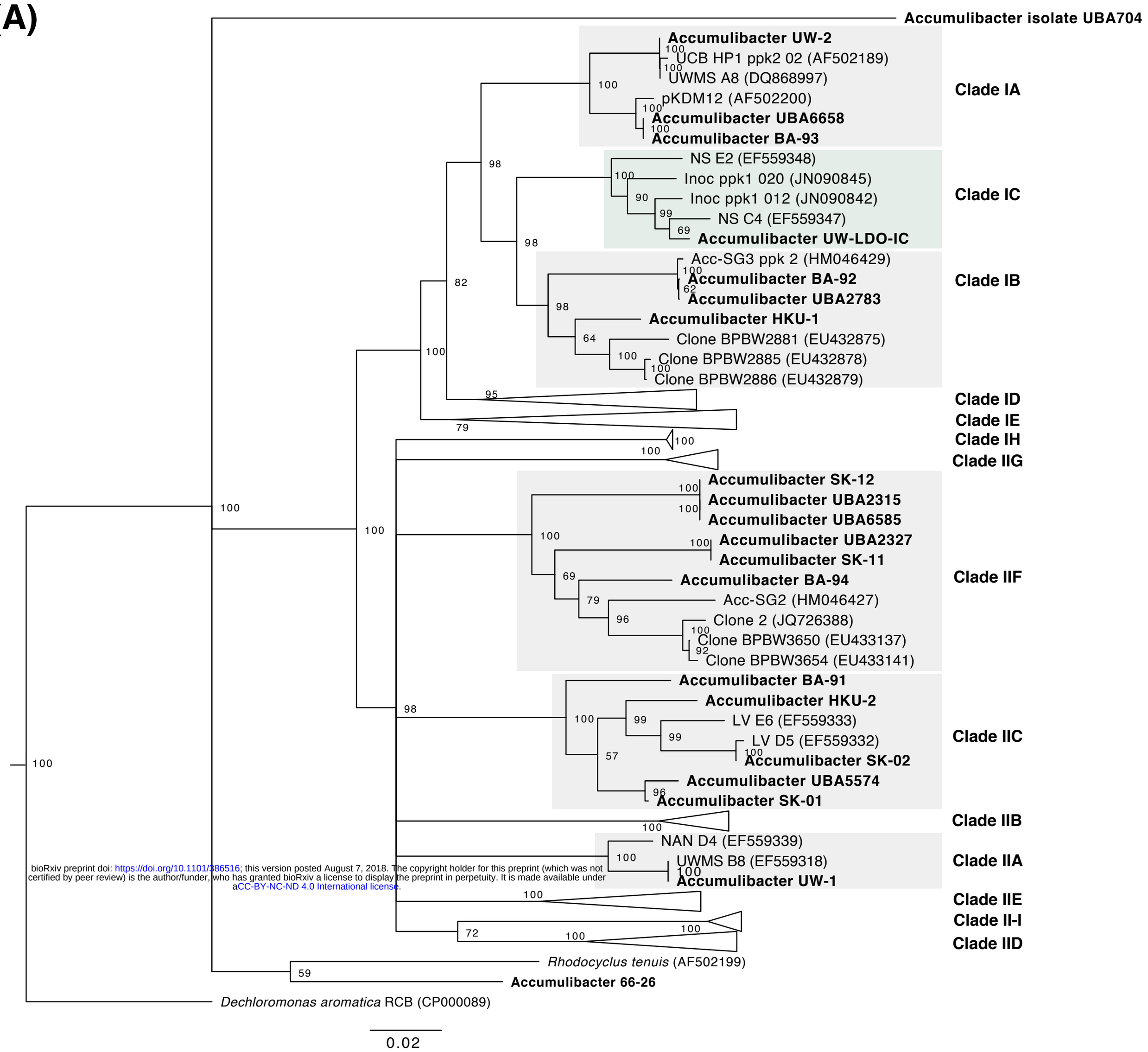

bioRxiv preprint doi: https://doi.org/10.1101/386516; this version posted August 7, 2018. The copyright holder for this preprint (which was not certified by peer review) is the author/funder, who has granted bioRxiv a license to display the preprint in perpetuity. It is made available under aCC-BY-NC-ND 4.0 International license.

(A)

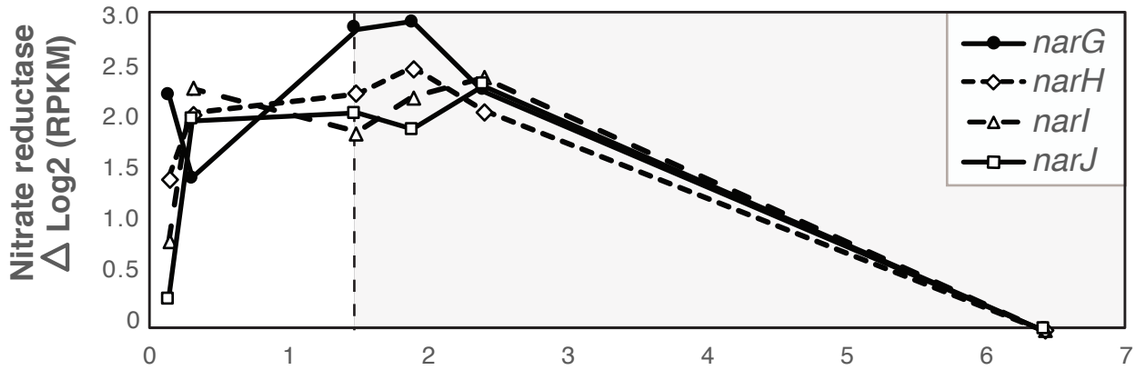
Nitrate reductase
Δ Log2 (RPKM)
narG
narH
narI
narJ

(B)

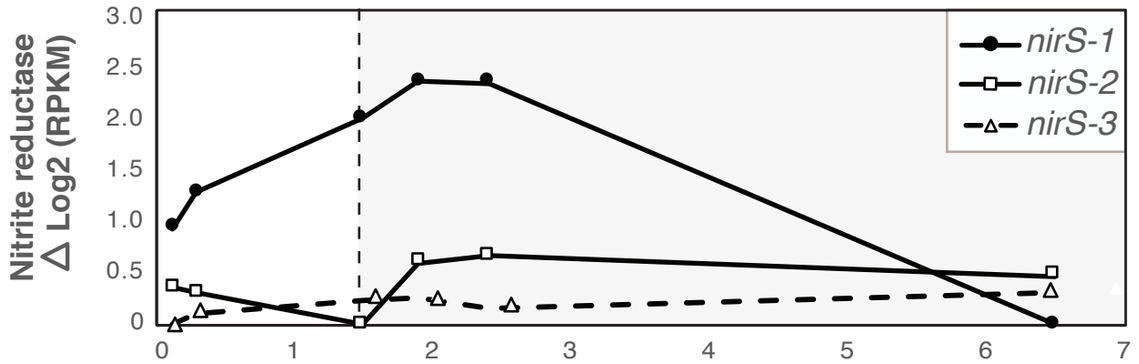
Nitrite reductase
Δ Log2 (RPKM)
nirS-1
nirS-2
nirS-3

(C)

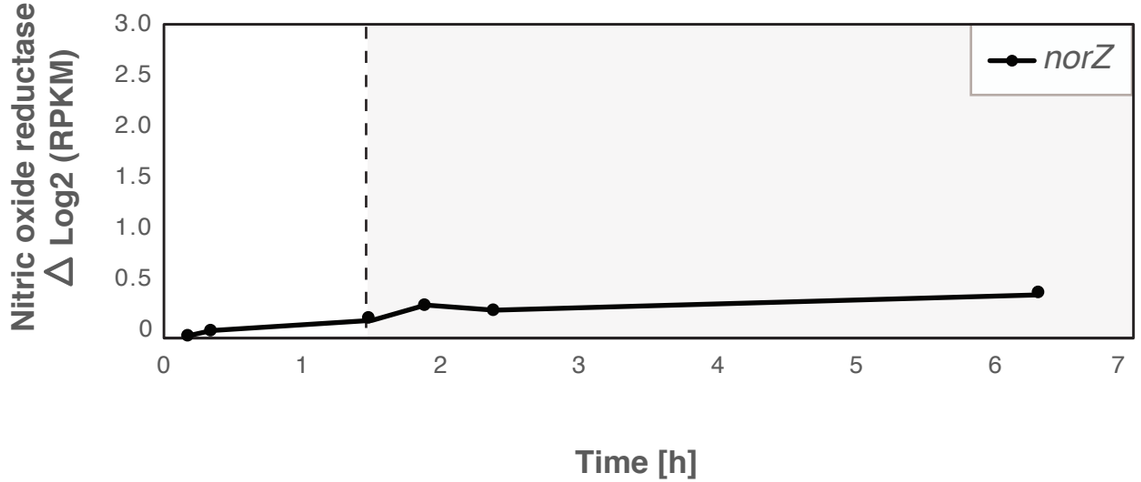
Nitric oxide reductase
Δ Log2 (RPKM)
norZ
Time [h]

(D)

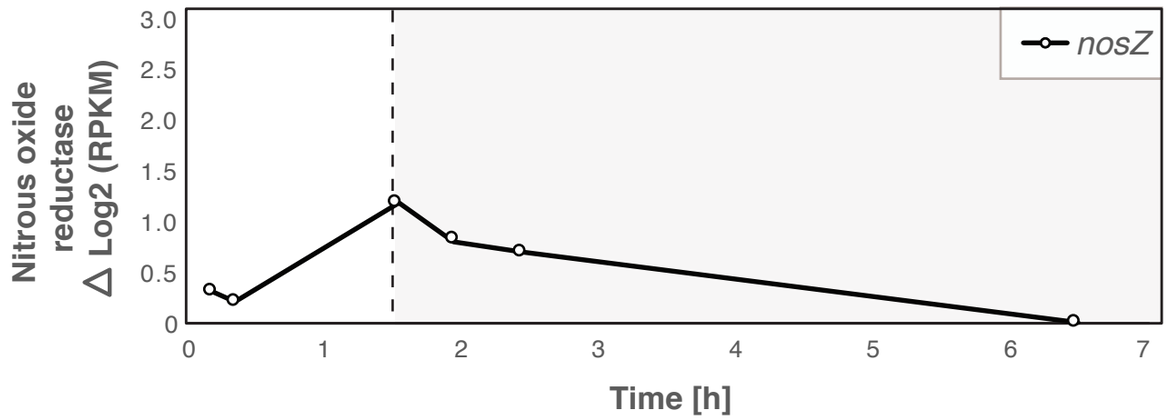
Nitrous oxide
reductase
Δ Log2 (RPKM)
nosZ
Time [h]

(E)

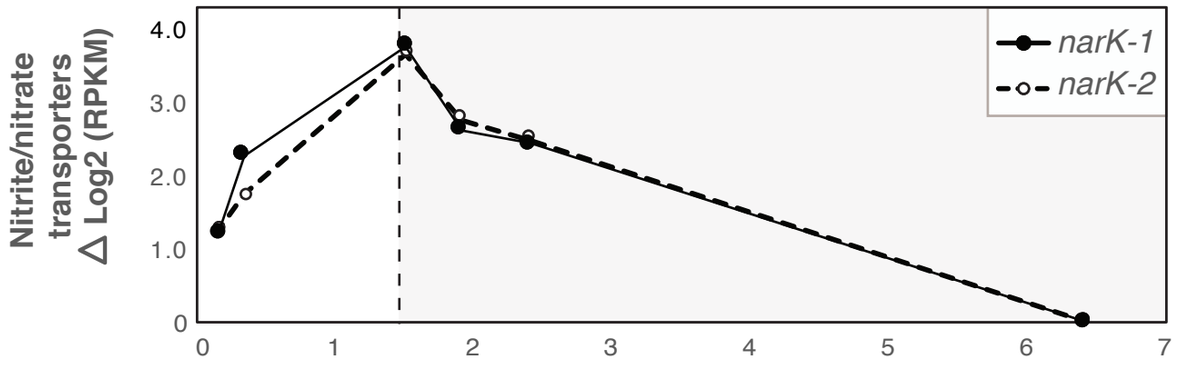
Nitrite/nitrate
transporters
Δ Log2 (RPKM)
narK-1
narK-2

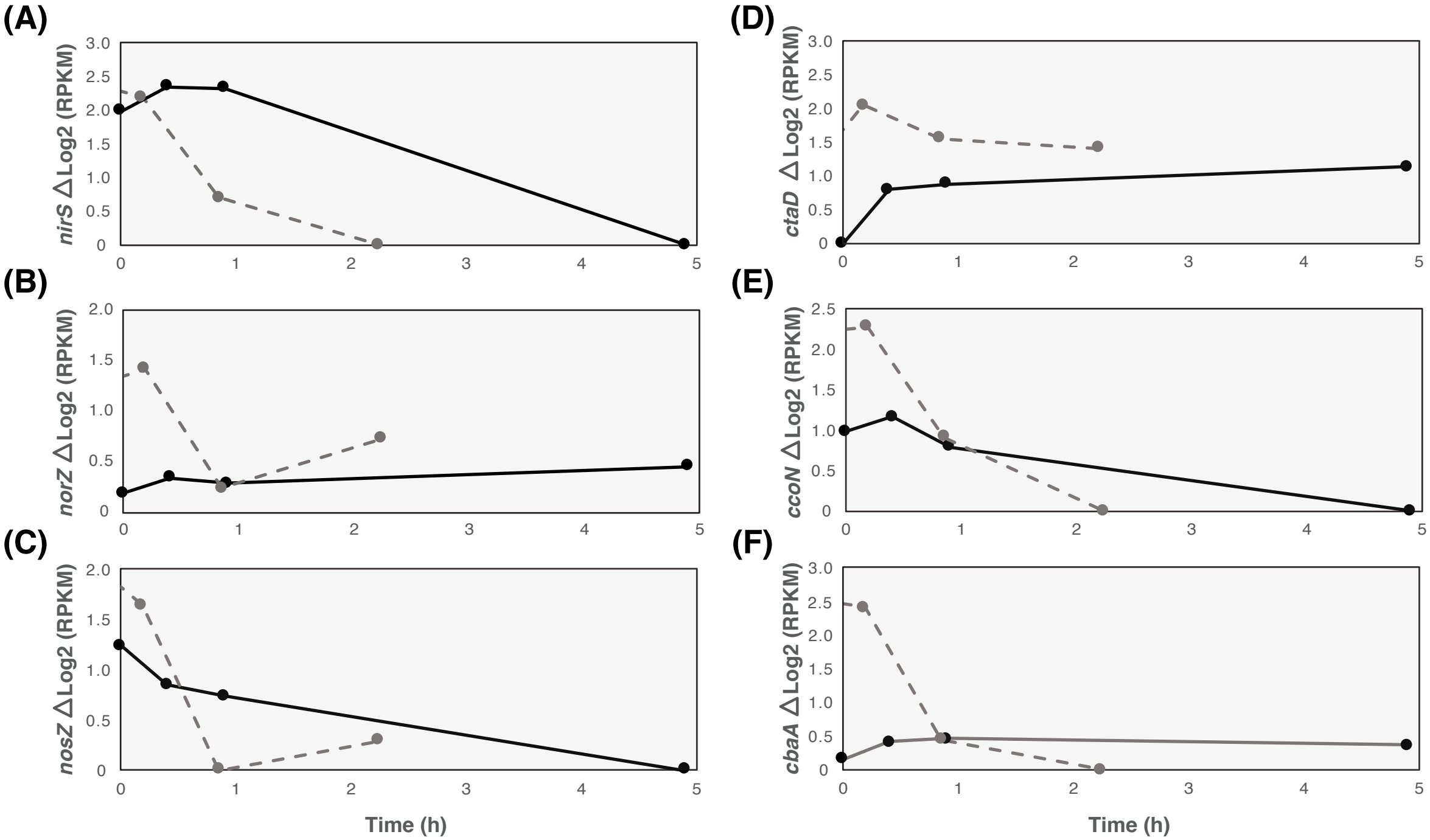
(A)
nirS ΔLog2 (RPKM)
(B)
norZ ΔLog2 (RPKM)
(C)
nosZ ΔLog2 (RPKM)
Time (h)
(D)
ctaD ΔLog2 (RPKM)
(E)
ccoN ΔLog2 (RPKM)
(F)
cbaA ΔLog2 (RPKM)
Time (h)

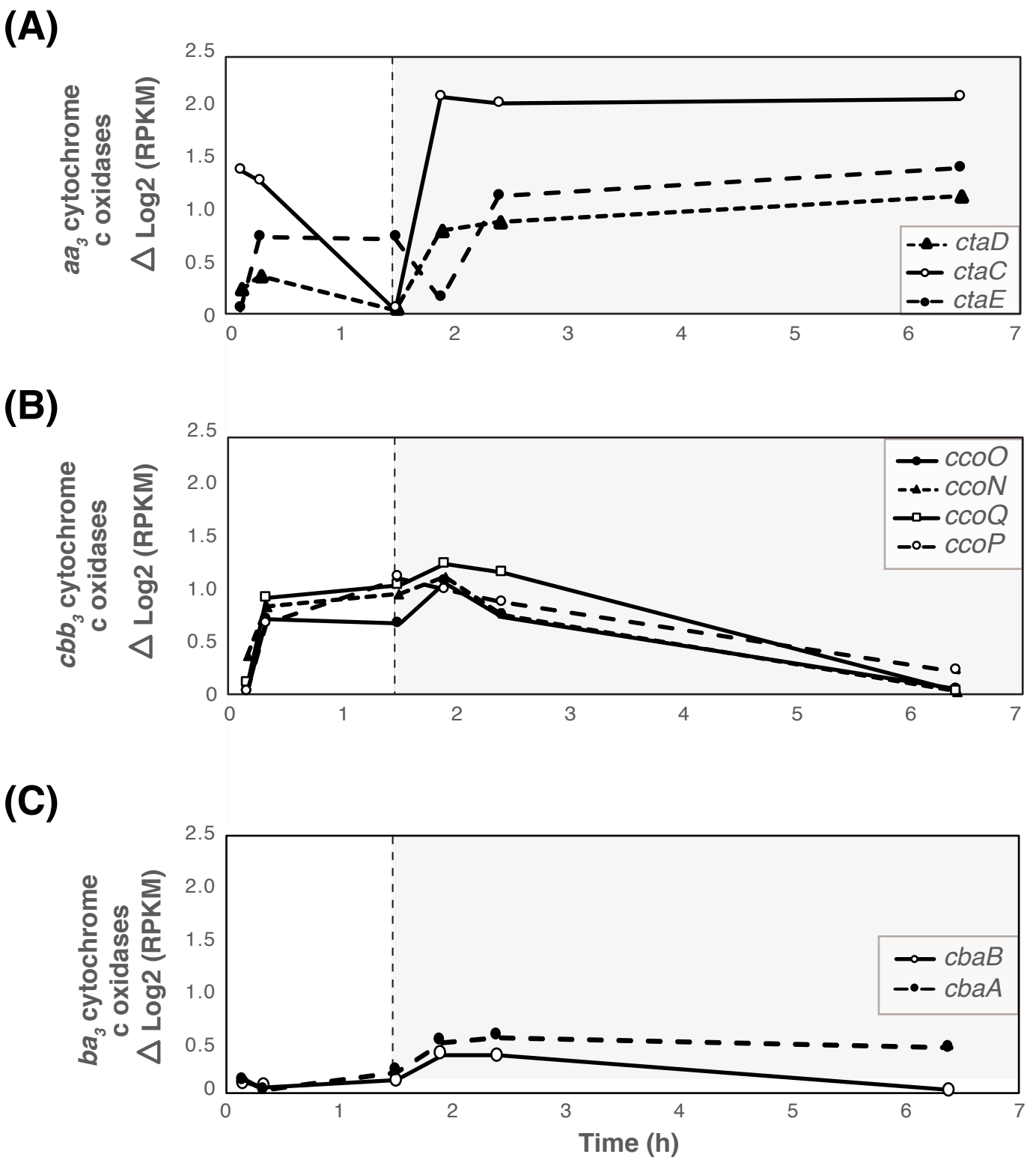
(A)
aa3 cytochrome c oxidases
Δ Log2 (RPKM)
ctaD
ctaC
ctaE
(B)
cbb3 cytochrome c oxidases
Δ Log2 (RPKM)
ccoO
ccoN
ccoQ
ccoP
(C)
ba3 cytochrome c oxidases
Δ Log2 (RPKM)
cbaB
cbaA
Time (h)

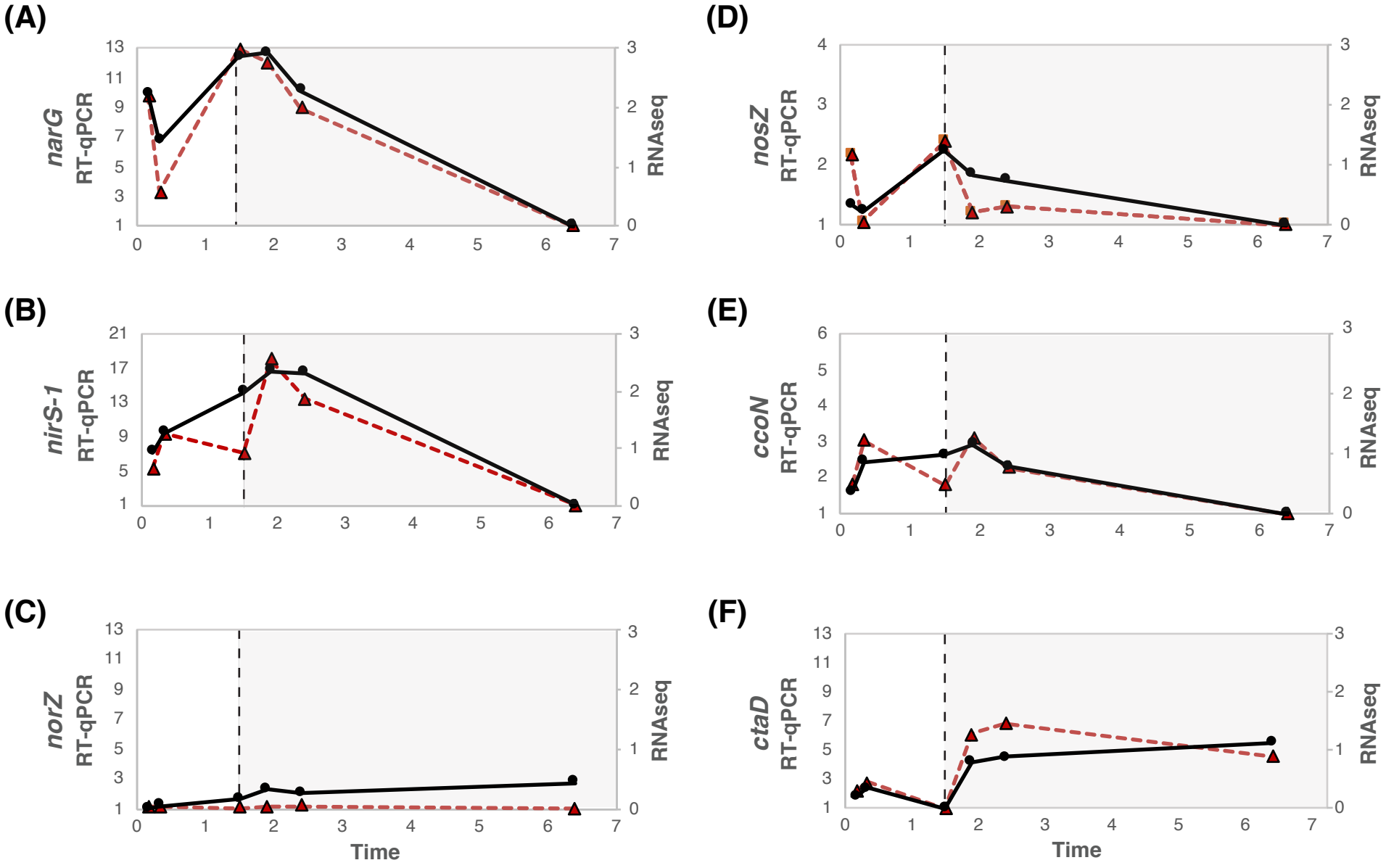
(A)
narG
RT-qPCR
RNAseq
(B)
nirS-1
RT-qPCR
RNAseq
(C)
norZ
RT-qPCR
RNAseq
Time
(D)
nosZ
RT-qPCR
RNAseq
(E)
ccoN
RT-qPCR
RNAseq
(F)
ctaD
RT-qPCR
RNAseq
Time

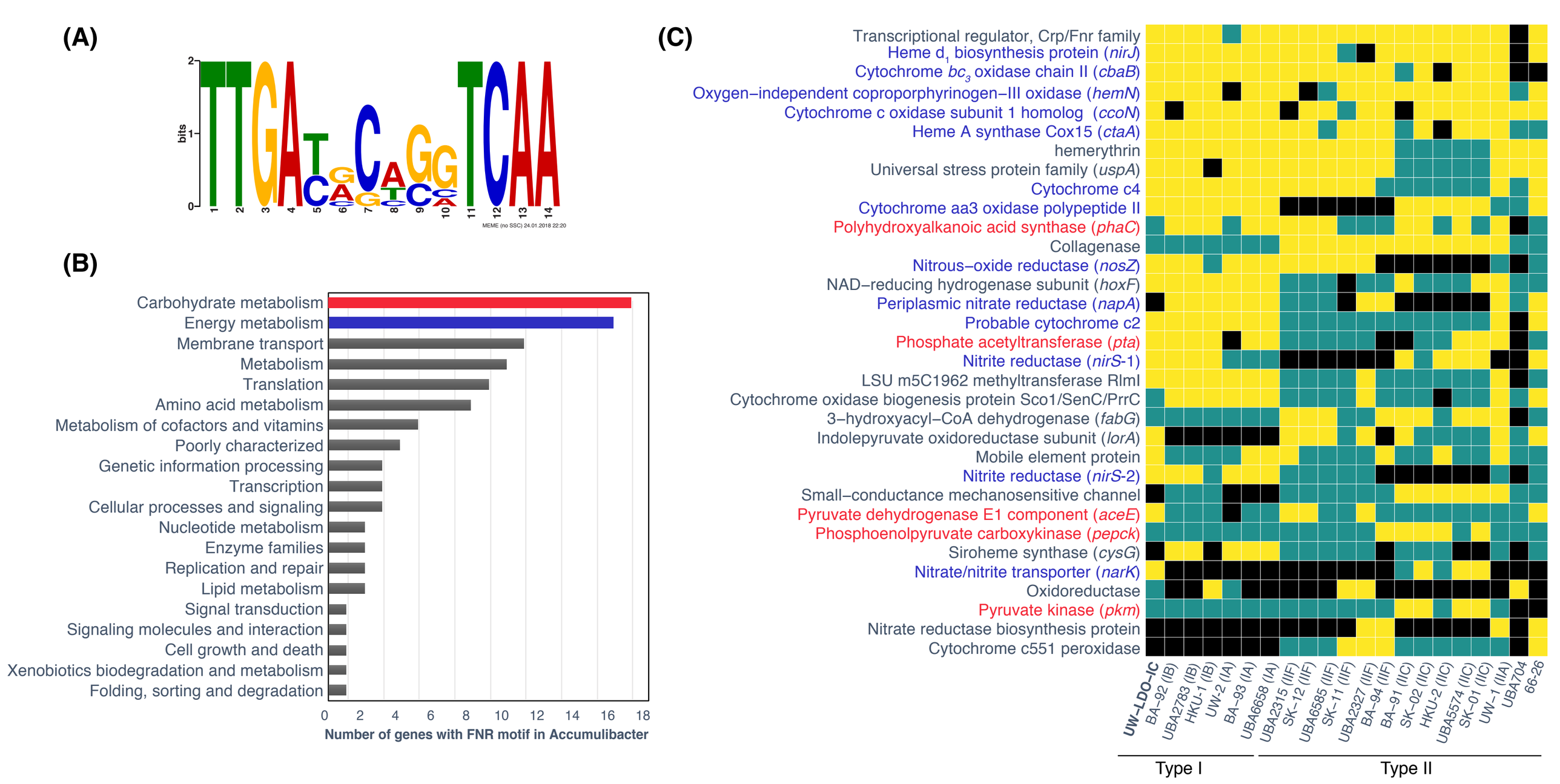
(A)
bits
MEME (no SSC) 24.01.2018 22:20
(B)
Carbohydrate metabolism
Energy metabolism
Membrane transport
Metabolism
Translation
Amino acid metabolism
Metabolism of cofactors and vitamins
Poorly characterized
Genetic information processing
Transcription
Cellular processes and signaling
Nucleotide metabolism
Enzyme families
Replication and repair
Lipid metabolism
Signal transduction
Signaling molecules and interaction
Cell growth and death
Xenobiotics biodegradation and metabolism
Folding, sorting and degradation
Number of genes with FNR motif in Accumulibacter
(C)
Transcriptional regulator, Crp/Fnr family
Heme d1 biosynthesis protein (nirJ)
Cytochrome bc3 oxidase chain II (cbaB)
Oxygen–independent coproporphyrinogen–III oxidase (hemN)
Cytochrome c oxidase subunit 1 homolog (ccoN)
Heme A synthase Cox15 (ctaA)
hemerythrin
Universal stress protein family (uspA)
Cytochrome c4
Cytochrome aa3 oxidase polypeptide II
Polyhydroxyalkanoic acid synthase (phaC)
Collagenase
Nitrous–oxide reductase (nosZ)
NAD–reducing hydrogenase subunit (hoxF)
Periplasmic nitrate reductase (napA)
Probable cytochrome c2
Phosphate acetyltransferase (pta)
Nitrite reductase (nirS-1)
LSU m5C1962 methyltransferase RlmI
Cytochrome oxidase biogenesis protein Sco1/SenC/PrrC
3–hydroxyacyl–CoA dehydrogenase (fabG)
Indolepyruvate oxidoreductase subunit (lorA)
Mobile element protein
Nitrite reductase (nirS-2)
Small–conductance mechanosensitive channel
Pyruvate dehydrogenase E1 component (aceE)
Phosphoenolpyruvate carboxykinase (pepck)
Siroheme synthase (cysG)
Nitrate/nitrite transporter (narK)
Oxidoreductase
Pyruvate kinase (pkm)
Nitrate reductase biosynthesis protein
Cytochrome c551 peroxidase
UW-LDO-IC
BA–92 (IB)
UBA2783 (IB)
HKU-1 (IB)
UW-2 (IA)
BA–93 (IA)
UBA6658 (IA)
UBA2315 (IIF)
SK–12 (IIF)
UBA6585 (IIF)
SK–11 (IIF)
UBA2327 (IIF)
BA–94 (IIF)
BA–91 (IIC)
SK–02 (IIC)
HKU-2 (IIC)
UBA5574 (IIC)
SK–01 (IIC)
UW–1 (IIA)
UBA704
66-26
Type I
Type II

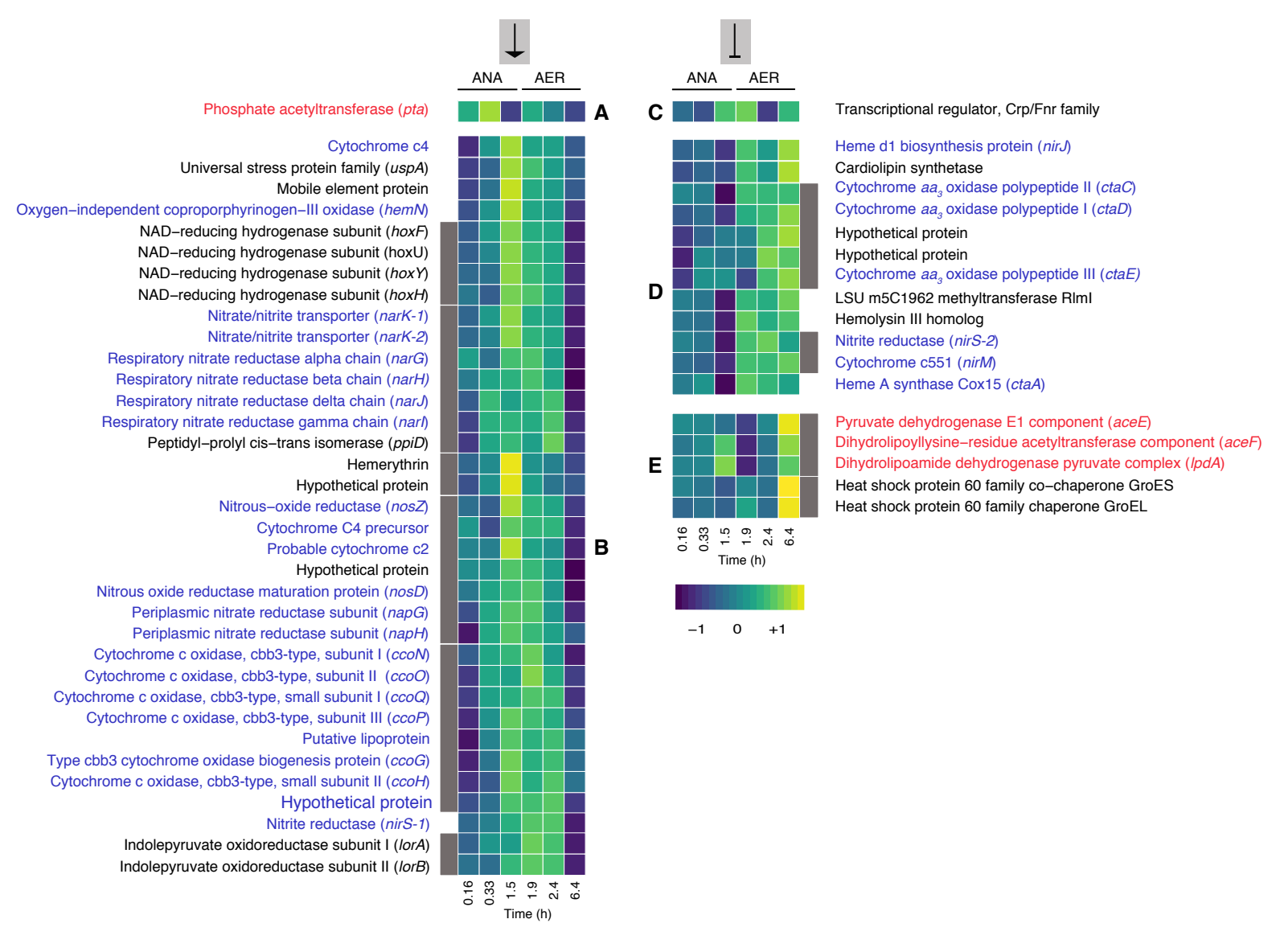
ANA
AER
Phosphate acetyltransferase (pta)
A
Cytochrome c4
Universal stress protein family (uspA)
Mobile element protein
Oxygen−independent coproporphyrinogen−III oxidase (hemN)
NAD−reducing hydrogenase subunit (hoxF)
NAD−reducing hydrogenase subunit (hoxU)
NAD−reducing hydrogenase subunit (hoxY)
NAD−reducing hydrogenase subunit (hoxH)
Nitrate/nitrite transporter (narK-1)
Nitrate/nitrite transporter (narK-2)
Respiratory nitrate reductase alpha chain (narG)
Respiratory nitrate reductase beta chain (narH)
Respiratory nitrate reductase delta chain (narJ)
Respiratory nitrate reductase gamma chain (narI)
Peptidyl−prolyl cis−trans isomerase (ppiD)
Hemerythrin
Hypothetical protein
Nitrous−oxide reductase (nosZ)
Cytochrome C4 precursor
Probable cytochrome c2
Hypothetical protein
Nitrous oxide reductase maturation protein (nosD)
Periplasmic nitrate reductase subunit (napG)
Periplasmic nitrate reductase subunit (napH)
Cytochrome c oxidase, cbb3-type, subunit I (ccoN)
Cytochrome c oxidase, cbb3-type, subunit II (ccoO)
Cytochrome c oxidase, cbb3-type, small subunit I (ccoQ)
Cytochrome c oxidase, cbb3-type, subunit III (ccoP)
Putative lipoprotein
Type cbb3 cytochrome oxidase biogenesis protein (ccoG)
Cytochrome c oxidase, cbb3-type, small subunit II (ccoH)
Hypothetical protein
Nitrite reductase (nirS-1)
Indolepyruvate oxidoreductase subunit I (lorA)
Indolepyruvate oxidoreductase subunit II (lorB)
B
0.16
0.33
1.5
1.9
2.4
6.4
Time (h)
ANA
AER
C
Transcriptional regulator, Crp/Fnr family
D
Heme d1 biosynthesis protein (nirJ)
Cardiolipin synthetase
Cytochrome aa3 oxidase polypeptide II (ctaC)
Cytochrome aa3 oxidase polypeptide I (ctaD)
Hypothetical protein
Hypothetical protein
Cytochrome aa3 oxidase polypeptide III (ctaE)
LSU m5C1962 methyltransferase RlmI
Hemolysin III homolog
Nitrite reductase (nirS-2)
Cytochrome c551 (nirM)
Heme A synthase Cox15 (ctaA)
E
Pyruvate dehydrogenase E1 component (aceE)
Dihydrolipoyllysine−residue acetyltransferase component (aceF)
Dihydrolipoamide dehydrogenase pyruvate complex (lpdA)
Heat shock protein 60 family co−chaperone GroES
Heat shock protein 60 family chaperone GroEL
0.16
0.33
1.5
1.9
2.4
6.4
Time (h)
−1
0
+1